Drake Passage gateway opening and Antarctic Circumpolar Current onset 31 Ma ago: The message of foraminifera and reconsideration of the Neodymium isotope record

F. Hodel, R. Grespan, M. de Rafélis, G. Dera, C. Lezin, E. Nardin, D. Rouby, M. Aretz, M. Steinnman, M. Buatier, et al.

Drake Passage Gateway opening and Antarctic Circumpolar Current onset 31 Ma ago: the message of foraminifera and reconsideration of the Neodymium isotope record

Hodel F.[1,2], Grespan R.[2], de Rafélis M.[2], Dera G.[2], Lezin C.[2], Nardin E.[2], Rouby D.[2], Aretz M.[2], Steinnman M.[1], Buatier M.[1], Lacan F.[3], Jeandel C.[3], Chavagnac V.[2]

[1] Laboratoire Chrono-Environnement, UMR6249 CNRS-UFC, 25000 Besançon, France
[2] Géosciences Environnement Toulouse (GET), UMR5563 Université de Toulouse/CNRS/IRD/Université Paul Sabatier, Observatoire Midi-Pyrénées, 31400 Toulouse, France
[3] Laboratoire d'Etudes en Géophysique et Océanographie Spatiale (LEGOS), Université de Toulouse/CNRS/CNES/IRD/Université Paul Sabatier), Observatoire Midi-Pyrénées, 31400 Toulouse, France

Abstract

The establishment of the Antarctic Circumpolar Current (ACC) is one of the most important events for both global oceanic circulation and climate of the Cenozoic. The onset of this major current hinges on the opening of two major oceanic passages, the Drake Passage and the Tasmanian gateways that connect Pacific, Atlantic and Indian oceans allowing a modern-like thermohaline circulation. For decades, the ACC onset has been considered as the trigger of the Oligocene glaciation at 33.7 Ma, which marks the beginning of the modern icehouse climate. Today, this scenario is debated. The main obstacle to evaluate the ACC influence on the Oligocene glaciation remains the ill-constrained timing of the Drake Passage gateway opening. Here, we analyse the geochemical composition and Sr isotope ratio of dated planktonic and benthic foraminifera from two IODP and ODP legs in the Southern Atlantic and Pacific oceans (SAO and PO, respectively) to assess the variability of seawater masses' chemical composition through time and to better constrain the timing of the Drake Passage gateway opening along the Eocene-Oligocene interval. These results, based on seawater paleo temperature (Mg/Ca molar ratios), redox (Ce/Ce* anomaly) and provenance ($^{87}Sr/^{86}Sr$) proxies, highlight a gradual seawater mass mixing between the SAO and PO from 31 Ma to 26 Ma. Combined with a reconsideration of the fossil fish teeth Neodymium isotope records, these geochemical tracers evidencing the SAO-PO interconnection depicts the Drake Passage gateway opening and deepening during this 31-26 Ma interval and thus, the timing of the ACC onset. Hence, antecedence of the Oligocene glaciation onset (at 33.7 Ma) relative to the ACC onset (31-26 Ma) implies that the ACC did not trigger the Oligocene glaciation and that the role of atmospheric pCO_2 should be further considered.

Key words: Drake Passage gateway, Oligocene glaciation, Antarctic Circumpolar Current, Climate, Paleoceanography, Foraminifera

1. Introduction

The inception of the modern icehouse climate goes back to a long-term Eocene global cooling, which ultimately led to the onset of the Oligocene glaciation at 33.7 Ma (Zachos et al., 2001). This pivotal climatic event of the Eocene-Oligocene transition (EOT) is recorded worldwide in the foraminifera geochemistry by a major shift toward higher $\delta^{18}O$ values (~+1.5 ‰), attesting to an abrupt seawater temperature decrease and ice-sheets formation (Coxall et al., 2005; Zachos et al., 2001). It is

nowadays consensual that the Eocene cooling resulted from a progressive atmospheric pCO_2 decrease, which in its turn lowered the global average oceanic temperature (DeConto and Pollard, 2003; Pagani et al., 2011; Ladant et al., 2014). Yet, the causes of the Oligocene glaciation itself are still debated. Two dominant theories have been suggested: the pCO_2 hypothesis and the ACC hypothesis. The CO_2 hypothesis states that the glaciation was triggered by an atmospheric pCO_2 decrease below a critical threshold (~750 ppm, DeConto et al., 2008; Ladant et al., 2014; Galeotti, et al., 2016), potentially combined with an orbital configuration that reduced polar seasonality (e.g. DeConto and Pollard, 2003; Coxall et al., 2005; Pagani et al., 2011; Ladant et al., 2014). The ACC hypothesis argues that the tectonic separation of Australia and South America from Antarctica led to the onset of the ACC. The ACC reduced heat transport to southern high latitudes by isolating Antarctica from the global oceanic circulation, thereby inducing the glaciation (Kennett, 1977; Kennett and Exon, 2004). Indeed, recent circulation model experiments have been able to generate strong southern hemisphere cooling in response to ACC onset (e.g. Sauermilch et al., 2019).

After decades of debate, the pCO_2 hypothesis is nowadays more and more admitted, notably since numerical climate and ocean circulation models have been able to simulate glaciation without involving the ACC onset (e.g. Ladant et al., 2014; Kennedy-Asser et al., 2020). However, the role of the ACC in the Eocene-Oligocene climate evolution remains largely misunderstood, especially because the timing of its onset is not well constrained. The onset of the ACC is driven by the opening of two major oceanic apertures around Antarctica, i.e. the Tasmanian and the Drake Passage gateways (Fig. 1). These gateways allowed for the ACC to form and to connect the Pacific, Atlantic and Indian oceans, leading to a modern-like thermohaline circulation (Stow, 2001; Stickley et al., 2004; Scher and Martin, 2006; Lagabrielle et al., 2009; Katz et al., 2011; Bijl et al., 2013; Scher et al., 2015; Sarkar et al., 2019). Stickley et al. (2004) showed that the Tasmanian gateway opened to deep oceanic circulation between 35.5 and 33.5 Ma. However, the timing of the Drake Passage gateway opening remains poorly constrained (Fig. 1), hindering any evaluation of the ACC influence on the Eocene-Oligocene climate (Scher, 2017).

Although numerous studies have focused on the Drake Passage gateway aperture, its opening is still a matter of debate. While some authors attest of a shallow corridor from 50 Ma (Livermore et al., 2005, 2007), most tectonic and sedimentology studies argue for its opening to a deep eastward circulation during the Oligocene (e.g. Latimer and Fillipelli, 2002; Lawver and Gahagan, 2003; Livermore et al., 2005, 2007; Brown et al., 2006; Eagles et al., 2006; Lagabrielle et al., 2009; Eagles and Jokat, 2014) (Fig. 1). Only a few studies using seawater geochemical tracers proposed an age for the Drake Passage gateway opening. Based on the Nd isotopes record of fossil fish teeth at Maud Rise (ODP Leg 113, site 689) and Agulhas Ridge (ODP Leg 177, site 1090), (see Fig. 1 for sites' location), Scher and Martin (2004, 2006) proposed a connection between the Pacific and Southern Atlantic oceans at *ca.* 41 Ma, evidenced by a gradual increase toward more radiogenic ε_{Nd} values at that time. Recently, Wright et al. (2018) showed a rather stable ε_{Nd} signal in fossil fish teeth from the Kerguelen Plateau (ODP Leg 119, sites 738 and 744, Fig. 1) between 33 and 23 Ma. This stability may reflect the absence of major paleoceanographic changes in the Southern Ocean during this interval, comforting the idea that the Drake Passage gateway was already open. However, the ε_{Nd} signature of bottom seawater recorded by fossil fish teeth can be strongly influenced by continental weathering fluxes (e.g. Lacan and Jeandel, 2005; Jeandel et al., 2007; Scher et al., 2011, 2014). This is particularly true for the Southern Ocean drilling sites, which are located near the Antarctica margin and thus potentially exposed to highly non-radiogenic Nd fluxes from the Proterozoic to Precambrian Antarctica's basement (e.g. Scher et al., 2011, 2014). Alternatively, Egan et al. (2013) showed a

decline in sponge $\delta^{30}Si$ values at 31.5 Ma from the Agulhas Ridge (site 1090, Fig. 1) that they interpreted as signing the final establishment of a deep-water circulation through the Tasmanian and Drake Passage gateways. Hence, if the Drake Passage gateway opened to deep circulation after the Tasmanian gateway, which opened *ca.* 35.5-33.5 Ma (Stickley et al., 2004), then its opening should have conditioned the ACC onset, potentially combined with westerlies alignment with the already opened Tasmanian gateway (Scher et al., 2015). Better constraining the timing of the Drake Passage gateway opening is thus fundamental to apprehend the ACC onset and to test its influence on the global climate (e.g. Scher, 2017).

Here, we establish robust temporal constraints on the Drake Passage gateway opening and the ACC onset by tracking Pacific/Atlantic seawater masses mixing over the Eocene-Oligocene interval. We selected benthic and planktonic foraminifera tests from the IODP Exp 320 (Hole 1334C) in the Pacific Ocean (PO) and the ODP Leg 113 (Hole 689B) in the Southern Atlantic Ocean (SAO) on which we performed major and trace element chemistry and Sr isotope ratio analysis (Fig. 1). The Hole 1334C has been chosen as a high quality oligotrophic Pacific Ocean endmember while the site 689B is ideally located in vicinity to the Drake Passage gateway outlet, thus allowing us to track PO inputs into the SAO following the gateway opening. Foraminifera use bioavailable elements of their living environment to build their calcitic test. For this reason, they are one of the most used pristine biomineral archive to assess past ocean chemistry since the pioneering works of Shackleton and Kennett (1975) and Palmer (1985). In this present work, we first verify that the geochemical features of the selected samples (e.g. major and trace element concentration and PAAS-normalised REE patterns) are in line with well-preserved seawater characteristics. Then, we use the Mg/Ca paleo-thermometer (Barker et al., 2005), the Ce anomaly [$Ce/Ce^{*}=Ce_N/(Pr_N \times (Pr_N/Nd_N))$] paleo-redox proxy (e.g. Bolhar et al., 2014; Kamber et al., 2014) and the $^{87}Sr/^{86}Sr$ isotope ratio (source tracer) to track temporal variations of seawater chemistry in Pacific and Southern Atlantic oceans during the EOT. By investigating these tracers in both planktonic and benthic foraminifera species, we aim to reconstruct both surface and bottom seawater chemical signatures in both PO and SAO, to decipher when water masses mixing between the PO and SAO occurred. Finally, we confront our results with the fossil fish teeth Nd isotope records available in the literature for the Pacific and the Southern oceans, which are commonly used in paleoceanographic studies. Altogether these investigations allow us to propose a more accurate timing for the Drake Passage gateway opening.

2. Methods

2.1. Sediments and foraminifera treatment

Based on the detailed core descriptions (Barker et al., 1988; Pälike et al., 2010), we selected 12 sediment fractions of the IODP Exp. 320 (Hole 1334C) in the PO and 10 from the ODP Leg 113 (Hole 689 B) in the SAO. A fraction of each sample was resuspended into Milli-Q water and filtrated back to back at 200 µm and 100 µm. Largest fractions (>200 µm and 200-100 µm if needed) were dried in a stove at 50 °C. Foraminifera were hand-picked under a binocular and separated according to planktonic and benthic species described in detailed shore-based studies (Barker et al., 1988; Pälike et al., 2010). We paid a particular attention to select solely entire, clean and well-preserved specimens devoid of any clay aggregate and oxyhydroxide patch or coating (Figs. 3 a, c, d). Back-scattered electrons (BSE) images of foraminifera tests and residues after chemical treatment were obtained

with using a JEOL JSM-6360LV electron microscope at the Géosciences Environnement Toulouse laboratory (Toulouse, France) operating at 20 kV.

In a clean laboratory, for each sample foraminifera fraction (between ~0.5 mg and ~20 mg depending of the foraminifera abundance) was rinsed with Milli-Q water, ultrasonized, and centrifuged 5 to 8 times. The supernatant was discarded between each cleaning step. This sample treatment allowed to remove any potential source of contamination such as clay particles or coccolithophores. Then, we added 500 µL of Milli-Q water to each cleaned foraminifera fraction, prior to stepwise dissolution by successively adding five times 100 µL aliquots of 1N acetic acid, resulting in 1 mL of a 0.5N acetic acid solution (e.g. Osborne et al., 2017). After ~10-20 minutes of reaction at room temperature, we centrifuged each tube during 8 minutes at 4000 rpm. The pipetted supernatant was then transferred in acid-cleaned Savillex beaker. Supernatants were dried on a hotplate at 70 °C. Residues were dissolved in 30 µL of double-distilled concentrated HCl and dried on a hotplate at 70 °C to remove any trace of acetates. Stock solutions were prepared with 2N double-distilled HNO_3. All acids used for sample preparation are trace element grade high purity acids. Quality controls of the described protocol are further presented in the results section 3.2. *Test preservation and contamination evaluation*.

2.2. Elemental chemistry

Aliquot of the stock solution corresponding to ~1 mg of foraminifera was pipetted and dried on a hotplate at 70 °C. 5 ml of 0.37N double-distilled HNO_3 solution doped with 1ppb In-Re solution were added to the residue. Major and trace element concentrations were measured using a Thermo Scientific Element XR HR-ICP-MS at the Observatoire Midi-Pyrénées (Toulouse, France). In and Re were used as internal standards during ICP-MS measurements to monitor instrumental drift during the course of the analyses. The instrument was calibrated using a synthetic multi-element solution routinely used by the Observatoire Midi-Pyrénées ICP-MS service. This calibration solution has been analysed with three different dilution factors, at the beginning and at the end of the analyses, in order to calibrate the instrument response and correct the drift along the analytical sequence. Oxide interferences (BaO^+ on Nd^+ and Eu^+, LREE on MREE and MREE on HREE, see table in Supplementary data 1) were then corrected. Oxide production rate was determined based on Cal-S standard material, the latter having similar matrix than our foraminifera. The precision and accuracy of ICP-MS analyses were assessed by measuring the reference materials GSJ CRM Jct-1 Giant Clam (*Tridacna gigas*, i.e. biocarbonate, National Institute of Advanced Industrial Science and Technology, Geological Survey of Japan, Inoue et al., 2004) and Cal-S (Calcite, Yeghicheyan et al., 2003). Because of the very low REE content of Jct-1, accurate REE concentrations cannot be measured through our "all-in-one" protocol for this standard (see the Tanaka et al., 2018 procedure combining isotopic dilution, REE co-precipitation and chromatographic separation). Therefore, we used Cal-S, which shows REE contents more comparable to our samples, for REE, Ca, Mg and Sr concentrations, and Jct-1 for Ca and Sr contents as well as for Sr isotope ratio analysis.

2.3. Sr isotope ratio analysis

Aliquot of each stock solution corresponding to ~0.5 mg of foraminifera was pipetted, transferred to a savillex beaker and dried on a hotplate at 70 °C. Sr was isolated from the matrix using liquid chromatographic columns loaded with Sr-Spec® ion selective resin (Pin et al., 2014). Sr isotope ratios were measured using a Thermo Scientific Triton Plus Thermal Ionization Mass Spectrometer (TIMS) at the Observatoire Midi-Pyrénées (Toulouse, France). Measured $^{87}Sr/^{86}Sr$ ratios are an average of 150 measurements of ion intensities following the static multi-collection mode normalized to $^{86}Sr/^{88}Sr$

= 0.1194. During the whole measurement period, NBS 987 standard was measured repetitively to precisely quantify the external reproducibility. The NBS 987 measurements gave a mean $^{87}Sr/^{86}Sr$ isotope ratio of 0.710286 ± 0.000009 (2σD, n=18). Thus we applied a correction of -0.000038 to all our measurements to fit with the reference NBS987 value of 0.710248. International and certified carbonate standards were processed alongside our sample series. We measured $^{87}Sr/^{86}Sr$ ratios of 0.709175 ± 14 (2σD, n=9) for Jct-1 and 0.706953 ± 12 (2σD, n=5) for Cal-S, in agreement with certified values of 0.709150± 0,000050 (Ohno and Hirata, 2007) and 0,709169 ± 0,000009 (Weber et al., 2017) and 0.706924 ± 0,000018 (Yeghicheyan et al., 2003), respectively.

3. Results

3.1. Age models

Both magnetostratigraphic and biostratigraphic data available for each site (Barker et al., 1988 for Hole 689B and Pälike et al., 2010 for Hole 1334C) were considered to build age models. Data for the Hole 689B have been updated to the GTS2012 (Gradstein et al., 2012). We used the R software (R Development Core Team., 2019, packages *changepoint* of Killick and Eckley, 2014 and *segmented* of Vito and Muggeo, 2003) in order to identify statistically robust regressions (of sedimentation rate) and to calculate the absolute age of each selected sample (Fig. 2). The 95 % confident interval of these regressions defines uncertainties on obtained ages (Fig. 2). The ages of the investigated samples range from 24.6 Ma to 38.2 Ma for Hole 1334C and from 25.5 Ma to 46 Ma for Hole 689B (Fig. 2).

3.2. Test preservation and contamination evaluation

After having carefully hand-picked the cleanest complete foraminifera tests, we performed Scanning Electron Microscopy (SEM) observations of both hand-picked foraminifera tests and residues after chemical treatment. Observations revealed very well-preserved tests devoid of significant calcite recrystallization (Fig. 3 a, b, c and d). The residues after foraminifera dissolution are clays, detrital (e.g. quartz grains, mica) and early-diagenetic phases (e.g. framboidal pyrite), with intact morphology and without evidence of partial dissolution. Thus, only carbonates were dissolved during the chemical treatment applied on the samples (Fig. 3).

In addition, for all fractions we modelled clay/calcium carbonate geochemical mixing using the major element compositions of planktonic and benthic foraminifera, in order to detect any potential clay contamination during chemical treatment (Supplementary data 2). Considering the major elements of clay minerals, e.g. notably Si and Al, the calculations always attest of less than 0.005 wt.% of potential clay contamination (less than 0.002% for more than 95 % of the samples, Fig. 4). In other words, for ~20 mg of foraminifera fraction, the maximum potential contribution of clay would be up to $1x10^{-3}$ mg, thus extremely limited. This confirms that the cleaning and chemical protocol used here allowed for proper extraction of the geochemical signature of foraminiferal biogenic calcite and thus to reconstruct the seawater chemistry at the time of the tests formation.

3.3. Foraminifera as past seawater chemistry recorder

3.3.1. Rare earth element contents and Ce anomaly temporal evolution

All analyzed foraminifera fractions from the two investigated oceans display smooth PAAS (Post Archean Australian Shales) normalized REE patterns typical of seawater (Fig. 5, Table 1 and Supplementary data 1). They are characterized by light rare earth elements (LREE) depletion

compared to heavy rare earth element (HREE), $(Pr/Yb)_N$ ratio ranging from 0.23 to 0.66 and 0.39 to 0.59 in PO and SAO, respectively. They also exhibit pronounced negative Ce/Ce* anomalies [$Ce/Ce^*=Ce_N/(Pr_N \times (Pr_N/Nd_N))$], Ce/Ce* ranging from 0.06 to 0.16 in PO and 0.21 to 0.58 into SAO (Fig. 5), as well as positive La/La* anomalies [$La/La^*=La_N/(Pr_N \times (Pr_N/Nd_N)^2)$], ranging from 1.30 to 2.26 in PO and 1.04 to 1.74 into SAO, both typical of modern seawater REE chemistry. This confirms the reliability of our chemical treatment to extract clean seawater signals. Moreover, the preservation of the both LREE depletion compared to MREE and HREE and the Ce/Ce* anomaly discards any diagenetic overprint (e.g. Deng et al., 2017).

Interestingly, the intensity of the Ce/Ce* anomaly in foraminifera from PO and SAO is not random and displays clear temporal evolutions though the investigated time period (Fig 6a). Both planktonic and benthic foraminifera from PO exhibit very negative and rather constant Ce/Ce* anomalies ranging from 0.06 to 0.16 between 35 and 26 Ma (Figs. 5a and 6a). In contrast, SAO foraminifera show much lower Ce/Ce* anomalies between 48 and 31 Ma, which slightly increase over that time period (e.g. Ce/Ce*=0.51 at 46 Ma and 0.43 at 31 Ma in benthic foraminifera, Fig. 6a). Then, these negative Ce anomalies strengthen, particularly in benthic foraminifera, until reaching similar values to PO foraminifera *ca.* 26 Ma (Ce/Ce* down to 0.21, Fig. 6a). In SAO benthic foraminifera, the La/La* positive anomaly strengthen after 29 Ma (La/La*<1.30 before 29 Ma and La/La*>1.65 afterwards, see Supplementary data 1).

3.3.2. Mg/Ca ratios temporal evolution

The foraminifera from the investigated sites display Mg/Ca molar ratios between 4.4 and 1.8 mmol/mol (Fig. 6b). From 34 Ma onwards, the Mg/Ca molar ratios of SAO and PO planktonic foraminifera decrease (Fig. 6b). Then, as for the Ce/Ce* anomaly, a major change occurs from 31 Ma onwards. After 31 Ma, Mg/Ca molar ratios of SAO planktonic foraminifera increase up to values similar to PO planktonic foraminifera (3.7 mmol/mol for SAO at 27.3 Ma and 3.9 mmol/mol for PO at 28.1 Ma, Fig. 6b in red and yellow, respectively). Contrary to planktonic foraminifera, Mg/Ca molar ratios of SAO benthic species do not increase but remain stable from 31 Ma (Mg/Ca molar ratios *ca.* 2.7 mmol/mol, Fig. 6b). Hence, SAO bottom and surface Mg/Ca signals, which were similar at 46, 44 and 31 Ma, start to dissociate from one another between 31 and 29 Ma.

3.3.3. Strontium isotope ratios

All analyzed foraminifera display $^{87}Sr/^{86}Sr$ isotope ratios similar to those reported in the literature for the Southern Ocean (Fig. 6c, Table 1 and Supplementary data 3). They follow a first order increasing trend towards more radiogenic values from *ca.* 37 Ma onwards, which is commonly interpreted as a consequence of increasing Sr continental weathering inputs associated with the Himalayan and Andean orogenies (e.g. Raymo and Ruddiman, 1992). At the 31 Ma tipping point previously identified in the Ce/Ce* and Mg/Ca records (Fig. 6a, b), a slight inflexion in the long-term rise of $^{87}Sr/^{86}Sr$ isotope ratios is noticeable for both SAO and PO foraminifera (Fig. 6c). This inflexion, highlighted by normalized derivatives of the $^{87}Sr/^{86}Sr$ curves (see Hodel et al., 2017, 2020 for a similar approach), is noticeable for both planktonic and benthic foraminifera which have been analyzed separately (Fig. 6c). It is also worth noticing that PO and SAO foraminifera $^{87}Sr/^{86}Sr$ isotope ratios slightly, but significantly, differ from one another prior to 31 Ma, before displaying statistically similar $^{87}Sr/^{86}Sr$ isotope ratios after 31 Ma (Fig. 6c). In details, PO foraminifera show more radiogenic $^{87}Sr/^{86}Sr$ isotope composition than SAO ones by up to 0.000043 *ca.* 38 Ma (i.e. 9 times higher than

the analytical error of isotopic measurements and 4.8 times higher than the internal reproducibility), before displaying statistically identical $^{87}Sr/^{86}Sr$ isotope ratios from 31 Ma onwards (Fig. 6c).

4. Discussion

4.1. PO and SAO water masses mixing between 31 Ma and 26 Ma

The Mg/Ca molar ratios, Ce/Ce* anomalies and $^{87}Sr/^{86}Sr$ isotope ratios of both planktonic and benthic foraminifera from both studied sites show clear temporal variations, all characterized by significant changes from *ca.* 31 Ma until *ca.* 26 Ma (Fig. 6). Understanding the reasons for these concomitant variations relies on identifying the processes that could have influenced past seawater chemical composition.

The integration of Mg ions in calcite during the foraminifera test precipitation being temperature dependant (favoured by high temperature), the Mg/Ca molar ratio in marine biocarbonates is extensively used to assess past seawater temperature evolutions: higher ratios signing higher temperature and *vice-versa* (e.g. Barker et al., 2005). In our samples, Mg/Ca molar ratios of SAO and PO planktonic foraminifera decrease from 34 Ma onwards, indicating a major seawater cooling at that time (Fig. 6b). This cooling is synchronous with the onset of the Oligocene glaciation at the EOT, evidenced by a marked increase of the $\delta^{18}O_{bf}$ values of benthic foraminifera worldwide (Zachos et al., 2001) (~+1.5 ‰, Fig. 8a), including those from the Hole 689 in the SAO (Kennett and Stott, 1990, in grey on Fig. 6b). Here, it is worth noting that both $\delta^{18}O_{bf}$ values of Kennett and Stott (1990) and our Mg/Ca molar ratios of benthic foraminifera denote similar bottom seawater temperature variations, attesting of the reliability of our Mg/Ca signals. It is nonetheless important to mention that our multi-species approach and our low sampling resolution can possibly mask additional complexities. Then, from 31 Ma onwards, Mg/Ca molar ratios of SAO planktonic foraminifera increase until reaching values similar to PO planktonic foraminifera *ca.* 27 Ma (in red and yellow respectively, Fig. 6b). This increase in Mg/Ca molar ratios of SAO planktonic foraminifera attests of a progressive warming of SAO surface waters between *ca.* 31 and *ca.* 27 Ma. In addition, Mg/Ca molar ratios of SAO planktonic and benthic foraminifera progressively become distinct from one another during this time interval, suggesting a SAO stratification with warmer sea-surface water masses than deep-seawater masses (Fig. 6b). This could sign the Drake Passage gateway opening. Indeed, a such decoupling between bottom and surface water masses is in line with modelling studies (e.g. Ladant et al., 2018; Zhang et al., 2020), which attests of a drastic decrease of the mixed layer depth (MLD) in the SAO following the Drake Passage gateway opening. These studies model an entirely mixed water column in the SAO before the Drake Passage gateway opening and a MLD at less than 200 m after the Drake Passage gateway opening (e.g. Ladant et al., 2018; Zhang et al., 2020). Therefore, the progressive surface waters warming that we observe between 31 Ma and 27 Ma possibly results from a more and more restricted MLD along the Drake Passage gateway opening and deepening, leading to the isolation of surface waters from cold bottom waters, hence promoting their warming (Fig. 7).

The hypothesis of water masses stratification in the SAO due to PO input following the Drake Passage gateway opening from 31 Ma and its deepening until at least 26 Ma is also supported by the Ce/Ce* anomaly temporal evolutions. The Ce/Ce* anomaly is one of the most used seawater redox and paleoredox proxy (e.g. Deng et al., 2017; Kamber et al., 2014; Osborne et al., 2017). Contrary to other REEs that are only tetravalent (with the exception of Eu), Ce is characterized by two redox states, III and IV. Under reducing conditions Ce^{3+} is soluble in water, while under oxidizing conditions CeO_2

precipitates. This Ce-oxide precipitation from seawater, i.e. Ce removal from the dissolved chemical load, induce negative Ce/Ce* anomalies (Ce/Ce* < 1, i.e. Ce depletion compared to its neighbouring REE, e.g. Zhang and Nozaki, 1996; Osborne et al., 2017). Hence, variations of the Ce/Ce* anomaly in seawater and so in foraminifera tests, can reflect dissolved pO_2 fluctuations (e.g. Zhang and Nozaki, 1996; Deng et al., 2017; Osborne et al., 2017). In parallel to the changes observed in the Mg/Ca molar ratios, the temporal evolution of Ce/Ce* anomalies shows a major decrease in SAO benthic foraminifera after the 31 Ma tipping point (Fig. 6a). Between 31 and 26 Ma, this pattern attests of a progressive oxygenation of SAO deep water up to a redox state similar to the PO seawater at *ca.* 26 Ma (Fig. 6a). This suggests a clear redox state homogenization between PO and SAO deep waters starting from 31 Ma and intensifying to 26 Ma, which argues for deep-water masses connexion between these two oceans during this time interval.

Finally, the $^{87}Sr/^{86}Sr$ ratios of analyzed foraminifera tests also testify important paleoceanographic changes through the studied interval (Fig. 6c). Despite similar rising trends, the $^{87}Sr/^{86}Sr$ ratios from the PO and SAO appear decoupled around 38-36 Ma (up to 0.000043 of difference, Fig. 6), before to merge together at 32 Ma and mark a rapid and global rise of $^{87}Sr/^{86}Sr$ ratios culminating at 31 Ma (Fig. 6c). The initial offset of $^{87}Sr/^{86}Sr$ ratios recorded between the two basins is quite enigmatic because the seawater $^{87}Sr/^{86}Sr$ ratio is generally considered as homogeneous worldwide. This is due to the long residence time of Sr in the ocean (~2.5 Myr) with respect to the global ocean mixing time (<1500 years) (see McArthur et al. 2020 for a review). Recent studies with high analytical precisions have well reported slight differences (±0.000010), both spatially and bathymetrically, in the $^{87}Sr/^{86}Sr$ isotope ratio of modern oceanic waters far from any continental sources (Huang et al., 2011; Mokadem et al., 2015). However, this isotopic heterogeneity is generally more typical of coastal domains where seawater and carbonate shells are more directly influenced by river and submarine groundwater Sr influxes (Jones et al., 2014; El Meknassi et al., 2018, 2020; Briard et al., 2020). Hence, this primarily calls to question the preservation of initial oceanic signature. Here, the mixing models based on the Si and Al concentrations of foraminifera tend to exclude any significant clay contamination and to validate our analytical protocol (Fig. 4). However, Sr exchanges with pore water and subsequent carbonate recrystallization during early-diagenesis cannot be totally excluded to explain the more radiogenic signature of the PO foraminifera before 32 Ma. Yet, this hypothesis does not fully explain neither why such processes only affected this Late Eocene interval, nor why planktonic and benthic foraminifera records from same core samples were differently affected. Moreover (1) we did not observe any evidence of such recrystallization in SEM observations (Fig. 3) and (2) foraminifera from site 1334C older than 32 Ma display typical seawater-like REE pattern characterized by very marked Ce anomalies (lowest Ce/Ce* ratio of all our sampling, Figs. 5 and 6), incompatible with pore waters influenced recrystallization, pore waters being characterized by the loss of the Ce anomaly of their originating seawater (e.g. Deng et al., 2017). In an alternative hypothesis validating the genuine oceanic origin of our $^{87}Sr/^{86}Sr$ records, the observed offset between SAO and PO foraminifera before 32 Ma would imply a partial decoupling of Sr reservoirs between the Pacific and Southern Atlantic oceans at that time. Although impossible to consider in a modern oceanic context dominated by global thermohaline circulation, such a mechanism was supposed at the geological time scale for periods with a net degree of water mass restriction and stratification between the oceanic basins (Banner 2004). This remains difficult to prove in our case but this potential restriction is not incoherent with recent numerical models suggesting a very active Weddell gyre isolating the Southern Atlantic domain in the Eocene, then vanishing when Pacific currents intruded the Drake Passage gateway (Toumoulin et al. 2020). If true, the spatial decoupling of Sr

isotopic patterns could be due to more radiogenic Sr supplies from proto-Andean and Himalayan reliefs in the Pacific and Indian oceans and low transfers towards Atlantic domains. Then, the merging of $^{87}Sr/^{86}Sr$ ratios that we observe could sign PO and SAO water masses homogenization from *ca.* 31 Ma, consistently with the temporal evolutions of Mg/Ca molar ratios and Ce/Ce* anomalies previously described (Fig. 6). This time was also marked by a global positive inflexion of the $^{87}Sr/^{86}Sr$ patterns possibly signing a global rise of continental weathering rates and radiogenic Sr flux to the ocean. But given (1) the slightness of this inflexion and (2) the 1 Ma decay between ours and compiled data, this hypothesis needs to be further scrutinized, notably by extensive high-resolution measurements of foraminiferal $^{87}Sr/^{86}Sr$ isotope ratio from Pacific, Atlantic (at low, equatorial and high latitudes) and Indian oceans during the Eocene-Oligocene interval.

Even if additional, notably higher resolution data are required, altogether Mg/Ca molar ratios, Ce/Ce* anomalies and Sr isotope ratios of PO and SAO foraminifera attest to a PO/SAO connexion from *ca.* 31 Ma and to an established deep-seawater flow *ca.* 26 Ma. This provides a better timing of the Drake Passage gateway opening, in line with the tectonic synthesis of Eagle and Jokat (2014) who conclude that the Drake Passage gateway likely opened to deep seawater flow between 30 and 26 Ma.

4.2. Reconsideration of the Neodymium isotope record

If our results and interpretations fit with the last tectonic synthesis of Eagle and Jokat (2014) and most of the other tectonic studies previously cited, they are contradictory with the most cited "chemical age" attributed to the Drake Passage gateway opening: 41 Ma inferred from the fossil fish teeth Neodymium isotope records (Scher and Martin 2006).

Besides tectonic and sedimentary studies, previous dating of the Drake Passage gateway opening through geochemical tracers is essentially based on the record of fossil fish teeth Neodymium isotopic compositions ($^{143}Nd/^{144}Nd$, expressed as $\varepsilon_{Nd}=((^{143}Nd/^{144}Nd_{sample}/^{143}Nd/^{144}Nd_{CHUR})-1)*10\ 000$; with CHUR standing for Chondrite Uniform Reservoir, $^{143}Nd/^{144}Nd=0.512638$; Bouvier et al., 2008). Nd has a short residence time of *ca.* 500 years in the ocean compared with to the global oceanic overturn of *ca.* 1500 years, making it sensitive to modification of seawater mass circulation (e.g. Scher and Martin, 2006; Scher et al., 2015). Because fossil fish teeth are considered to record bottom seawater REE content, their Nd isotope compositions are used to track seawater masses through geological time (e.g. Martin and Haley, 2000; Scher and Martin, 2004). However, seawater Nd isotope composition has to be carefully reconsidered due to its high sensitivity to continental-weathering fluxes to the ocean, particularly in proximal oceanic domains (e.g. Frank, 2002; Lacan and Jeandel, 2005; Jeandel et al., 2007; Jeandel, 2016).

At present, the most consensual "isotopic age" for the Drake Passage gateway opening is around 41 Ma (Scher and Martin 2006). This hypothesis relies on an ε_{Nd} increase toward more radiogenic values in fish teeth from the Agulhas Ridge (from ~ -8 ε_{Nd} at *ca.* 41 Ma to -6 ε_{Nd} at *ca.* 39 Ma, site 1090, Fig. 8b in blue) and to a much slighter extent at Maud Rise (site 689, Scher and Martin, 2004, Fig. 8b in red). This Nd isotope excursion is interpreted as signing Pacific radiogenic seawater inflow (in yellow) to Southern Ocean from 41 Ma (Fig. 8b). Nonetheless, compiled data for the Kerguelen Plateau, which is supposed to have also been strongly affected by Pacific seawater inputs through the Drake Passage gateway do not show such an increasing ε_{Nd} trend starting at 41 Ma. Then, from *ca.* 37 Ma to *ca.* 34 Ma, a second ε_{Nd} increase is noticeable in fossil fish teeth from for Agulhas Ridge and Maud Rise, as well as in those of the Kerguelen Plateau (Fig. 8b). The latter is also interpreted as enhanced Pacific radiogenic seawater inputs related to the Drake Passage gateway opening (Scher

and Martin, 2004, 2006). On the other hand, recent fish teeth Nd isotope data from Huck et al. (2017), which enlarge the Kerguelen plateau ε_{Nd} record to the early Eocene, attest that ε_{Nd} values gradually increased from ~ -10 ε_{Nd} at 50 Ma to ~ -7 ε_{Nd} at 35 Ma (Fig. 8b, in green). This suggests that either (1) the Drake Passage gateway opened to significant seawater flow as soon as the early Eocene (*ca.* 50 Ma), or (2) this trend reflects the contribution of an additional Nd source, other than radiogenic Pacific seawater input into Southern Ocean.

If some tectono-sedimentary studies attest of a possible shallow opening of the Drake Passage gateway at the early-Eocene (e.g. Livermore et al., 2005, 2007), most of them argues for its opening to eastward deep circulation during the Oligocene (Latimer and Fillipelli, 2002; Lawver and Gahagan, 2003; Eagles et al., 200; Livermore et al., 2005, 2007; Brown et al., 2006; Lagabrielle et al., 2009; Eagles and Jokat, 2014) (Fig. 1). Hence, geological evidences of these studies do not support a significant connection between Pacific and Southern oceans through the Drake Passage gateway as early as 50 Ma to explain the ε_{Nd} increasing trend recorded in fish teeth from the Kerguelen Plateau (Fig. 8b). This supports the hypothesis of an additional Nd source, potentially continental weathering fluxes from Antarctica related the Eocene-Oligocene cooling and associated ice-sheet formation (Fig 8a). Indeed, potential Antarctica's weathering regime evolutions have to be carefully considered in the interpretation of Southern Ocean fossil fish teeth ε_{Nd} record because of (1) the highly non-radiogenic Nd isotope composition of Antarctica's lithologies bordering the Southern Atlantic and Indian oceans (e.g. core top sediments reach -21.3 ε_{Nd} near the Prydz Bay, Roy et al., 2007; Van de Flierdt et al., 2007; Scher et al., 2014), (2) the vicinity of Antarctica to the Southern Ocean sites investigated for Eocene-Oligocene paleoceanographic studies (Kerguelen Plateau, Maud Rise and Agulhas Ridge, Fig. 1), and (3) the isolated setting of the Southern Ocean before the Drake and Tasmanian gateways deep opening.

Punctually, brief episodes of intense continental export associated with glacial pulses, e.g. the PrOM-event (*ca.* 37 Ma) and EOT (*ca.* 34 Ma) glaciations, are marked by negative ε_{Nd} excursions of 1.5 to 3 ε_{Nd} units of amplitude in fossil fish teeth from the Kerguelen Plateau (Scher et al., 2011, 2014) (Fig. 8). In these studies, as well as in Huck et al (2017), authors attributed these excursions to brutal changes in weathering regime (glacial dynamic onset and debacle episodes) of Archean-Proterozoic-Early Phanerozoic Antarctica's lithologies (Roy et al., 2007; Musumeci et al., 2000), delivering highly non-radiogenic Nd flux to the ocean, hence drawing down the ε_{Nd} record toward less radiogenic values in fossil fish teeth at that time. This clearly demonstrates the high sensitivity of the fish teeth Nd record to variations of continental weathering fluxes, which can produce ε_{Nd} shift of a similar amplitude compared to those imputed to oceanic circulation changes (e.g. potential Pacific input from *ca.* 41 Ma and 37 Ma, Scher and Martin, 2006) (Fig. 8b). This questions the effect of longer climate phenomenon and the associated weathering regime changes on the ε_{Nd} fish teeth record, notably along the Eocene cooling that led to the Oligocene glaciation.

Indeed, the Eocene cooling drastically impacted Antarctica's continental weathering regimes, as evidenced by the emergence of illite to the detriment of smectite - signing hydrolysis and so chemical weathering weakening - and by the concomitant occurrence of detrital chlorite in the Maud Rise and Agulhas Ridge sedimentary piles (notably from 41-40 Ma, Ehrmann and Mackensen, 1992; Diekmann et al., 2004). Thus, the progressive reduction of chemical inputs from Antarctica along the Eocene cooling likely resulted in a decrease of highly non-radiogenic Nd fluxes from Antarctica during this time interval. This is consistent with, and could explain, the progressive increasing trend toward more radiogenic ε_{Nd} values of fish teeth from the Kerguelen plateau from the early-Eocene (~

-10 ε_{Nd} at 50 Ma) to the EOT (e.g. ~ -7 ε_{Nd} at 35 Ma) (Fig. 8b, in green). Similarly, increasing ε_{Nd} trends observed from 41 Ma at the Agulhas Ridge (and Maud Rise) and from 37 Ma at Maud Rise, the Agulhas Ridge and the Kerguelen Plateau (Fig. 8b), could also result from a diminution of continental weathering fluxes from Antarctica, coupled with, or rather than, Drake Passage gateway opening and Pacific seawater inputs (Scher and Martin, 2004, 2006). Indeed, this two-stepwise increase of the Southern Ocean ε_{Nd} record is synchronous with the two main glacial events preceding the EOT glaciation, namely the first icecaps evidences at Antarctica *ca.* 42-41.5 Ma (Tripati et al., 2005) accompanied by the clay mineralogical evolutions previously mentioned *ca.* 41 Ma, and the PrOM-event *ca.* 37 Ma (Fig. 8).

This high sensitivity of the Southern Ocean ε_{Nd} fish teeth record to both punctual and long-term Antarctica's weathering fluxes evolutions, opens up the door to the idea of a buffering of the Southern Ocean (here Kerguelen Plateau, Maud Rise and Agulhas Ridge) fish teeth Nd isotope compositions by highly non-radiogenic continental weathering fluxes from Antarctica. This "buffering hypothesis" is also consistent with the slight ε_{Nd} offset (~0.5 ε_{Nd}) noticed by Wright et al. (2018) between the sites 744 (less radiogenic and closer to Antarctica) and 748 (more radiogenic and further away from Antarctica) which could testify of a latitudinal gradient of this buffering. In addition, the vicinity of the Maud Rise and the Kerguelen Plateau sites with Antarctica could explain why no major changes have been identified in the ε_{Nd} fish teeth records from these localities after 33 Ma (Wright et al., 2018). Climate and so continental weathering having stabilized after the EOT glaciation onset, this stable ε_{Nd} record could be the expression of the ε_{Nd} buffering by Antarctica's weathering fluxes, which could have hindered the detection of the Drake Passage gateway opening Nd isotope signal (i.e. Pacific radiogenic water input). Therefore, the Nd isotope fish teeth records from high latitude Southern Ocean sites might represent an Antarctica's continental weathering history rather than a Southern Ocean's seawater masses history.

If the Southern Ocean Nd isotope record was indeed partially buffered by Antarctica continental weathering fluxes, identifying Pacific and Southern oceans mixing would rely on the Pacific record. The latter had a much more radiogenic ε_{Nd} signature than any other oceans during the Eocene (Fig. 8b). Thus, an abrupt collapse in the ε_{Nd} temporal evolution of PO fossil fish teeth should occur in case of mixing with Southern Ocean non-radiogenic seawater. An extensive fossil fish teeth records have been made available by Scher et al. (2015) for the PO (Fig. 8b, in yellow). A first drop in ε_{Nd} values of fossil fish teeth from the Western Tasmanian Margin (site 1168) occurs between 36 Ma and 33 Ma (down to -7 ε_{Nd} while the Pacific endmember shows much more radiogenic values from -4 to -5 ε_{Nd}) possibly signing the Tasmanian gateway opening (Stickley et al., 2004). Then, Scher et al. (2015) evidenced a major ε_{Nd} collapse in the Southern Pacific Ocean record (sites 1124, 1168 and 1172) from *ca.* 30 Ma (Fig. 8b). Authors interpreted this collapse as signing the ACC onset and Pacific-Southern Ocean connection following westerlies alignment with a previously opened Tasmanian gateway (deep seawater circulation through the Tasmanian gateway starting from 35.5 to 33.5 Ma, Stickley et al., 2004). In this study, authors involved the migration of the northern margin of the Tasmanian gateway into the zone of the westerlies as the trigger for the ACC because they consider the Drake Passage gateway as being already open by the late Eocene (*ca.* 41-37 Ma, Scher and Martin, 2006). However, as previously developed, this Eocene opening is based on the Southern Ocean fish teeth Nd isotopes record (at Agulhas Ridge and Maud Rise), and can also be related to decreases of weathering rates on Antarctica in response to the Eocene cooling (particularly the first icecap formation *ca.* 42-41 Ma and the PrOM-event *ca.* 37 Ma, e.g. Tripati et al., 2005; Scher et al., 2014, Fig. 8) rather than to paleoceanographic changes. Alternatively, Scher et al. (2015) did not discard

the influence of far field tectonic in that ε_{Nd} collapse, notably the influence of the Drake Passage gateway opening. Interestingly, this major collapse of ε_{Nd} values at Pacific sites is synchronous with the SAO-PO connection evidenced from *ca.* 31 Ma (with a probable deepening to 26 Ma) by our Mg/Ca, Ce/Ce* and Sr isotopes data from Maud Rise (site 689) and the Pacific Ocean (site 1334) (Figs. 6 and 8). We thus propose that this ε_{Nd} collapse more likely signs the ACC onset following the Drake Passage gateway opening rather than, or combined with, westerlies alignment with the Tasmanian gateway (Scher et al., 2015). This statement is in adequacy with other geochemical tracers such as Si isotopes on sponge tests that attests of a PO-SAO connection from *ca.* 31.5 Ma (Egan et al., 2013), as well as most tectonic and sedimentary studies, which argue for an Oligocene Drake Passage gateway opening to deep seawater circulation (see above).

4.3. Implication for the global climate and ocean circulation

Here, we evidence a progressive Drake Passage gateway opening to significant seawater flow starting from 31 Ma and its deepening to 26 Ma. In this case, the Drake Passage gateway opening postdates the Tasmanian gateway aperture (35.5-33.5 Ma, Stickley et al., 2004). Hence, the ACC onset has necessarily relied on the Drake Passage gateway opening and so has likely been initiated during the 31-26 Ma interval. Within this temporal framework, the antecedence of the Oligocene glaciation onset (33.7 Ma) relative to the ACC onset, possibly from 31 Ma and strengthening from 31 Ma to 26 Ma, confirms that the ACC alone did not trigger the Oligocene glaciation. This reinforces the pCO_2 hypothesis, which states that the Oligocene glaciation resulted from atmospheric pCO_2 drawdowns below threshold value of ~750 ppm (DeConto and Pollard, 2003; Pagani et al., 2011; Ladant et al., 2014; Galeotti et al., 2016) under favourable orbital configurations (i.e. low eccentricity and low-amplitude change in obliquity resulting in dampened seasonality, Coxall et al., 2005). However, mechanisms involved in the Eocene atmospheric pCO_2 decrease are still debated. It has been hypothesized that even a shallow opening of the Drake Passage gateway could have influenced the evolution of pCO_2 prior to the Oi-1 and the onset of the ACC (Eagles et al., 2006). However, increases in continental weathering are arguably the most important mechanism for this long-term atmospheric pCO_2 drawdown (e.g. Raymo and Ruddiman, 1992; Zachos et al., 1999; Ravizza and Peucker-Ehrenbrink, 2003; Van der Flierdt, 2011; Elsworth et al., 2017). Yet, the mechanisms involved in that continental weathering increase remain ill-constrained. Additionally, the Antarctic ice sheet itself may have provided a positive feedback by impacting the ocean circulation, chemistry, and productivity and so atmospheric pCO_2 (e.g. Miller et al., 2009) while the albedo effect of the growing Antarctic ice-sheet could have contributed to cooler seawater temperature (e.g. DeConto et al., 2007). Therefore, to better constrain the mechanisms involved in the Eocene-Oligocene pCO_2 drawdown and the triggering of the Oligocene glaciation itself remain a prime topic for further studies to better constrain the Earth's global climate feedbacks.

The Antarctica's gateways opening is also of a major interest not only for ACC onset itself but for the whole thermohaline circulation, which cannot initiate without southern connections between Pacific, Atlantic and Indian oceans (e.g. Stow, 2001; Katz et al., 2011; Straume et al., 2020; Toumoulin et al., 2020). Indeed, "the modern four-layer ocean structure and increased export of Northern Component Water to the South Atlantic has been related to the development of the Antarctic Circumpolar Current" (in Vahlenkamp et al., 2018), the latter having been allowed by the Drake and Tasmanian gateways opening (e.g. Stow, 2001; Katz et al., 2011). The seawater masses stratification that we evidence through Mg/Ca molar ratios and Ce/Ce* anomalies and that we interpret as signing the Drake Passage gateway opening in the 31-26 Ma interval could have participated to the establishment

of the Antarctic Bottom Water (AABW) (Katz et al., 2011; Stow, 2001). Such proto-AABW formation could then have promoted the Atlantic Meridional Overturning Circulation (AMOC), hence initiating a global thermohaline circulation (Katz et al., 2011; Elsworth et al., 2017). Therefore, the date that we propose in this contribution for the Drake Passage gateway opening and ACC initiation also possibly signs the premises of a modern-like thermohaline circulation during the 31-26 Ma time interval.

5. Conclusion

In summary, Mg/Ca molar ratios, Ce/Ce* anomalies and $^{87}Sr/^{86}Sr$ isotope compositions acquired on both benthic and planktonic foraminifera attest to a connection between the PO and SAO from 31 Ma onwards, reflecting the Drake Passage gateway opening and its progressive deepening to 26 Ma. These results, in adequacy with the last tectonic-sedimentary synthesis on the Drake Passage gateway and with our revised interpretation of the Pacific ε_{Nd} record (ε_{Nd} collapse ~30 Ma), provide a better timing of the Drake Passage gateway opening. Since the Tasmanian gateway was already open to deep seawater circulation at that time, the Drake Passage gateway opening between 31 Ma and 26 Ma likely led to the establishment of the ACC during this time interval. Also, this opening of the Drake Passage gateway likely played a crucial role in the modern-like thermohaline circulation onset and the AABW establishment. Finally, the antecedence of the Oligocene glaciation onset (33.7 Ma), relative to the Drake Passage gateway opening to deep seawater circulation, and ACC onset (31-26 Ma) confirms that the ACC alone did not trigger the Oligocene glaciation even if it may have played and still plays a central role into the stabilization of the following icehouse climate. Thus, the abrupt Oligocene glaciation onset would have been triggered by pCO_2 drawdown below threshold values (below ~750 ppm), whether or not coupled with favourable orbital configurations, as previously proposed and modelled. To identify the contributions of the various forcing leading to major pCO_2 decline, such as tectonic, continental weathering, AMOC and nutrient supply, and to understand their influence on the Earth's climate dynamics is thus fundamental as much for the past as for the future.

References

- Banner, J.L., 2004. Radiogenic isotopes: systematics and applications to earth surface processes and chemical stratigraphy. Sedimentology 65, 141–194. https://doi.org/10.1016/S0012-8252(03)00086-2
- Barker, P.E., Kennett, J.P., et al., 1988. Proceedings of the Ocean Drilling Program, 113 Scientific Reports. Proc. Ocean Drill. Progr. 113. doi:10.2973/odp.proc.ir.113.106.1988
- Barker, S., Cacho, I., Benway, H., Tachikawa, K., 2005. Planktonic foraminiferal Mg/Ca as a proxy for past oceanic temperatures: a methodological overview and data compilation for the Last Glacial Maximum. Quat. Sci. Rev. 24, 821–834. https://doi.org/10.1016/J.QUASCIREV.2004.07.016
- Barker, P.F., Filippelli, G.M., Florindo, F., Martin, E.E., Scher, H.D., 2007. Onset and role of the Antarctic Circumpolar Current. Deep Sea Res. Part II Top. Stud. Oceanogr. 54, 2388–2398. https://doi.org/10.1016/j.dsr2.2007.07.028
- Barrera, E., Barron, J., Halliday, A., 1991. Strontium Isotope Stratigraphy of the Oligocene-Lower Miocene Section at Site 744, Southern Indian Ocean, in: Proceedings of the Ocean Drilling Program, 119 Scientific Results. Ocean Drilling Program. https://doi.org/10.2973/odp.proc.sr.119.211.1991
- Barth, M.G., McDonough, W.F., Rudnick, R.L., 2000. Tracking the budget of Nb and Ta in the continental crust. Chem. Geol. 165, 197–213. https://doi.org/10.1016/S0009-2541(99)00173-4
- Bijl, P.K., Bendle, J.A.P., Bohaty, S.M., Pross, J., Schouten, S., Tauxe, L., Stickley, C.E., McKay, R.M., Röhl, U., Olney, M., Sluijs, A., Escutia, C., Brinkhuis, H., Expedition 318 Scientists, E. 318, 2013. Eocene cooling

linked to early flow across the Tasmanian Gateway. Proc. Natl. Acad. Sci. U. S. A. 110, 9645–50. https://doi.org/10.1073/pnas.1220872110

- Bolhar, R., Kamber, B.S., Moorbath, S., Fedo, C.M., Whitehouse, M.J., 2004. Characterisation of early Archaean chemical sediments by trace element signatures. Earth Planet. Sci. Lett. 222, 43–60. https://doi.org/10.1016/j.epsl.2004.02.016

- Borrelli, C., Cramer, B.S., Katz, M.E., 2014. Bipolar Atlantic deepwater circulation in the middle-late Eocene: Effects of Southern Ocean gateway openings. Paleoceanography 29, 308–327. https://doi.org/10.1002/2012PA002444

- Bouvier, A., Vervoort, J.D., Patchett, P.J., 2008. The Lu-Hf and Sm-Nd isotopic composition of CHUR: Constraints from unequilibrated chondrites and implications for the bulk composition of terrestrial planets. Earth Planet. Sci. Lett. 273, 48–57. https://doi.org/10.1016/j.epsl.2008.06.010

- Briard J., Pucéat E., Vennin E., Daëron M., Chavagnac V., Jaillet R., Merle D., de Rafélis M., 2020. Seawater paleotemperature and paleosalinity evolution in neritic environments of the Mediterranean margin during the Miocene: insights from combined isotope analysis of bivalve shells. Palaeogeography, Palaeoclimatology, Palaeoecology, 10.1016/j.palaeo.2019.109582.

- Brown, B., Gaina, C., Müller, R.D., 2006. Circum-Antarctic palaeobathymetry: Illustrated examples from Cenozoic to recent times. Palaeogeogr. Palaeoclimatol. Palaeoecol. 231, 158–168. https://doi.org/10.1016/J.PALAEO.2005.07.033

- Coxall, H.K., Wilson, P.A., Pälike, H., Lear, C.H., Backman, J., 2005. Rapid stepwise onset of Antarctic glaciation and deeper calcite compensation in the Pacific Ocean. Nature 433, 53–57. https://doi.org/10.1038/nature03135

- Cramer, B.S., Toggweiler, J.R., Wright, J.D., Katz, M.E., Miller, K.G., 2009. Ocean overturning since the late cretaceous: Inferences from a new benthic foraminiferal isotope compilation. Paleoceanography 24. https://doi.org/10.1029/2008PA001683

- DeConto, R.M., Pollard, D., 2003. Rapid Cenozoic glaciation of Antarctica induced by declining atmospheric CO2. Nature 421, 245–249. https://doi.org/10.1038/nature01290

- DeConto, R., Pollard, D., Harwood, D., 2007. Sea ice feedback and Cenozoic evolution of Antarctic climate and ice sheets. Paleoceanography 22. https://doi.org/10.1029/2006PA001350

- DeConto, R.M., Pollard, D., Wilson, P.A., Pälike, H., Lear, C.H., Pagani, M., 2008. Thresholds for Cenozoic bipolar glaciation. Nature 455, 652–656. https://doi.org/10.1038/nature07337

- Deer, W.A., Howie, R.A., Zussman, J., 2013. Introduction to the Rock-forming Minerals. London.

- Deng, Y., Ren, J., Guo, Q., Cao, J., Wang, H., Liu, C., 2017. Rare earth element geochemistry characteristics of seawater and porewater from deep sea in western Pacific. Sci. Rep. 7, 16539. https://doi.org/10.1038/s41598-017-16379-1

- Diekmann, B., G. Kuhn, R. Gersonde, and A. Mackensen 2004, Middle Eocene to early Miocene environmental changes in the sub-Antarctic Southern Ocean: Evidence from biogenic and terrigenous patterns at ODP Site 1090, Global Planet. Change, 40, 295– 313.

- Eagles, G., Livermore, R., Morris, P., 2006. Small basins in the Scotia Sea: The Eocene Drake Passage gateway. Earth Planet. Sci. Lett. 242, 343–353. https://doi.org/10.1016/J.EPSL.2005.11.060

- Eagles, G., Jokat, W., 2014. Tectonic reconstructions for paleobathymetry in Drake Passage. Tectonophysics 611, 28–50. https://doi.org/10.1016/J.TECTO.2013.11.021

- Egan, K.E., Rickaby, R.E.M., Hendry, K.R., Halliday, A.N., 2013. Opening the gateways for diatoms primes Earth for Antarctic glaciation. Earth Planet. Sci. Lett. 375, 34–43. https://doi.org/10.1016/J.EPSL.2013.04.030

- Ehrmann, W.U., Mackensen, A., 1992. Sedimentological evidence for the formation of an East Antarctic ice sheet in Eocene/Oligocene time. Palaeogeogr. Palaeoclimatol. Palaeoecol. 93, 85–112. https://doi.org/10.1016/0031-0182(92)90185-8

- El Meknassi, S., Dera, G., Cardone, T., De Rafélis, M., Brahmi, C., Chavagnac, V., 2018. Sr isotope ratios of modern carbonate shells: Good and bad news for Chemostratigraphy. Geology 46, 1003–1006. https://doi.org/10.1130/G45380.1

- El Meknassi, S., Dera, G., De Rafélis, M., Brahmi, C., Lartaud, F., Hodel, F., Jeandel, C., Menjot, L., Mounic, S., Henry, M., Besson, P., Chavagnac, V., 2020. Seawater 87Sr/86Sr ratios along continental margins: Patterns and processes in open and restricted shelf domains. Chem. Geol. 558, 119874. https://doi.org/10.1016/j.chemgeo.2020.119874

- Elsworth, G., Galbraith, E., Halverson, G., Yang, S., 2017. Enhanced weathering and CO2 drawdown caused by latest Eocene strengthening of the Atlantic meridional overturning circulation. Nat. Geosci. 10, 213–216. https://doi.org/10.1038/ngeo2888

- Frank, M., 2002. Radiogenic isotopes: Tracers of past ocean circulation and erosional input. Rev. Geophys. 40, 1-1-1–38. https://doi.org/10.1029/2000RG000094

- Galeotti, S., DeConto, R., Naish, T., Stocchi, P., Florindo, F., Pagani, M., Barrett, P., Bohaty, S.M., Lanci, L., Pollard, D., Sandroni, S., Talarico, F.M., Zachos, J.C., 2016. Antarctic Ice Sheet variability across the Eocene-Oligocene boundary climate transition. Science (80-.). 352, 76–80. https://doi.org/10.1126/science.aab0669

- Gradstein, F.M., Ogg, J.G., Schmitz, M.D., Ogg, G.M. (Eds.), 2012. The Geologic Time Scale 2012, Elsevier. ed.

- Grenier, M., Jeandel, C., Lacan, F., Vance, D., Venchiarutti, C., Cros, A., Cravatte, S., 2013. From the subtropics to the central equatorial Pacific Ocean: Neodymium isotopic composition and rare earth element concentration variations. J. Geophys. Res. Ocean. 118, 592–618. https://doi.org/10.1029/2012JC008239

- Hague, A.M., Thomas, D.J., Huber, M., Korty, R., Woodard, S.C., Jones, L.B., 2012. Convection of North Pacific deep water during the early Cenozoic. Geology 40, 527–530. https://doi.org/10.1130/G32886.1

- Hammer, Ø., Harper, D.A.T., Ryan, P.D., 2001. PAST: Paleontological statistics software package for education and data analysis. Palaeontol. Electron. 4, 9.

- Hathorne, E.C., Stichel, T., Brück, B., Frank, M., 2014. Rare earth element distribution in the Atlantic sector of the Southern Ocean: The balance between particle scavenging and vertical supply. Mar. Chem. 177, 157–171. https://doi.org/10.1016/j.marchem.2015.03.011

- Hodel, F., Macouin, M., Triantafyllou, A., Carlut, J., Berger, J., Rousse, S., Ennih, N., Trindade, R.I.F., 2017. Unusual massive magnetite veins and highly altered Cr-spinels as relics of a Cl-rich acidic hydrothermal event in Neoproterozoic serpentinites (Bou Azzer ophiolite, Anti-Atlas, Morocco). Precambrian Res. 300, 151–167. https://doi.org/10.1016/j.precamres.2017.08.005

- Hodel, F., Macouin, M., Trindade, R.I.F., Araujo, J.F.D.F., Respaud, M., Meunier, J.F., Cassayre, L., Rousse, S., Drigo, L., Schorne-Pinto, J., 2020. Magnetic Properties of Ferritchromite and Cr-Magnetite and Monitoring of Cr-Spinels Alteration in Ultramafic and Mafic Rocks. Geochemistry, Geophys. Geosystems 21. https://doi.org/10.1029/2020GC009227

- Huang, K.-F., You, C.-F., Chung, C.-H., Lin, I.-T., 2011. Nonhomogeneous seawater Sr isotopic composition in the coastal oceans: A novel tool for tracing water masses and submarine groundwater discharge. Geochemistry, Geophys. Geosystems 12, n/a-n/a. https://doi.org/10.1029/2010gc003372

- Huck, C.E., van de Flierdt, T., Bohaty, S.M., Hammond, S.J., 2017. Antarctic climate, Southern Ocean circulation patterns, and deep water formation during the Eocene. Paleoceanography 32, 674–691. https://doi.org/10.1002/2017PA003135

- Inoue M., Nohara M., Okai T., Suzuki A. and Kawahata H. (2004) Concentrations of trace elements in carbonate reference materials coral JCp-1 and giant clam JCt-1 by inductively coupled plasma-mass spectrometry. Geostandards and Geoanalytical Research, 28, 411–416.

- Jeandel, C., Arsouze, T., Lacan, F., Téchiné, P., Dutay, J.C., 2007. Isotopic Nd compositions and concentrations of the lithogenic inputs into the ocean: A compilation, with an emphasis on the margins. Chem. Geol. 239, 156–164. https://doi.org/10.1016/j.chemgeo.2006.11.013
- Jeandel, C., 2016. Overview of the mechanisms that could explain the 'Boundary Exchange' at the land–ocean contact. Philos. Trans. R. Soc. A Math. Phys. Eng. Sci. 374, 20150287. https://doi.org/10.1098/rsta.2015.0287
- Jones, M.T., Gislason, S.R., Burton, K.W., Pearce, C.R., Mavromatis, V., Pogge von Strandmann, P.A.E., Oelkers, E.H., 2014. Quantifying the impact of riverine particulate dissolution in seawater on ocean chemistry. Earth Planet. Sci. Lett. 395, 91–100. https://doi.org/10.1016/j.epsl.2014.03.039
- Kamber, B.S., Greig, A., Collerson, K.D., 2005. A new estimate for the composition of weathered young upper continental crust from alluvial sediments, Queensland, Australia. Geochim. Cosmochim. Acta 69, 1041–1058. https://doi.org/10.1016/j.gca.2004.08.020
- Kamber, B.S., Webb, G.E., Gallagher, M., 2014. The rare earth element signal in Archaean microbial carbonate: Information on ocean redox and biogenicity. J. Geol. Soc. London. 171, 745–763. https://doi.org/10.1144/jgs2013-110
- Katz, M.E., Cramer, B.S., Toggweiler, J.R., Esmay, G., Liu, C., Miller, K.G., Rosenthal, Y., Wade, B.S., Wright, J.D., 2011. Impact of Antarctic Circumpolar Current development on late Paleogene ocean structure. Science 332, 1076–9. https://doi.org/10.1126/science.1202122
- Kennedy-Asser, A.T., Lunt, D.J., Valdes, P.J., Ladant, J.-B., Frieling, J., Lauretano, V., 2020. Changes in the high-latitude Southern Hemisphere through the Eocene–Oligocene transition: a model–data comparison. Clim. Past 16, 555–573. https://doi.org/10.5194/cp-16-555-2020
- Kennett, J., Stott, L., 1990. Proteus and Proto-Oceanus: ancestral Paleogene oceans as revealed from Antarctic stable isotopic results; ODP Leg 113. Proc. Ocean Drill. Progr. 113.
- Kennett, J.P., 1977. Cenozoic evolution of Antarctic glaciation, the circum-Antarctic Ocean, and their impact on global paleoceanography. J. Geophys. Res. 82, 3843–3860. https://doi.org/10.1029/JC082i027p03843
- Kennett, J.P., Exon, N.F., 2004. Paleoceanographic evolution of the Tasmanian Seaway and its climatic implications. American Geophysical Union (AGU), pp. 345–367. https://doi.org/10.1029/151GM19
- Killick, R., Eckley, I.., 2014. Changepoint: An R Package for Changepoint Analysis. J. Stat. Softw. 58, 1–19.
- Lacan, F., Jeandel, C., 2005. Neodymium isotopes as a new tool for quantifying exchange fluxes at the continent-ocean interface. Earth Planet. Sci. Lett. 232, 245–257. https://doi.org/10.1016/j.epsl.2005.01.004
- Ladant, J.-B., Donnadieu, Y., Lefebvre, V., Dumas, C., 2014. The respective role of atmospheric carbon dioxide and orbital parameters on ice sheet evolution at the Eocene-Oligocene transition. Paleoceanography 29, 810–823. https://doi.org/10.1002/2013PA002593
- Ladant, J.B., Donnadieu, Y., Bopp, L., Lear, C.H., Wilson, P.A., 2018. Meridional Contrasts in Productivity Changes Driven by the Opening of Drake Passage. Paleoceanogr. Paleoclimatology 33, 302–317. https://doi.org/10.1002/2017PA003211
- Lagabrielle, Y., Goddéris, Y., Donnadieu, Y., Malavieille, J., Suarez, M., 2009. The tectonic history of Drake Passage and its possible impacts on global climate. Earth Planet. Sci. Lett. 279, 197–211. https://doi.org/10.1016/j.epsl.2008.12.037
- Latimer, J.C., Filippelli, G.M., 2002. Eocene to Miocene terrigenous inputs and export production: geochemical evidence from ODP Leg 177, Site 1090. Palaeogeogr. Palaeoclimatol. Palaeoecol. 182, 151–164. https://doi.org/10.1016/S0031-0182(01)00493-X
- Lawver, L.A., Gahagan, L.M., 2003. Evolution of Cenozoic seaways in the circum-Antarctic region. Palaeogeogr. Palaeoclimatol. Palaeoecol. 198, 11–37. https://doi.org/10.1016/S0031-0182(03)00392-4
- Livermore, R., Nankivell, A., Eagles, G., Morris, P., 2005. Paleogene opening of Drake Passage. Earth Planet. Sci. Lett. 236, 459–470. https://doi.org/10.1016/J.EPSL.2005.03.027
- Livermore, R., Hillenbrand, C.-D., Meredith, M., Eagles, G., 2007. Drake Passage and Cenozoic climate: An open and shut case? Geochemistry, Geophys. Geosystems 8, n/a-n/a. https://doi.org/10.1029/2005GC001224

- Martin, E.E., Haley, B.A., 2000. Fossil fish teeth as proxies for seawater Sr and Nd isotopes. Geochim. Cosmochim. Acta 64, 835–847. https://doi.org/10.1016/S0016-7037(99)00376-2
- Martinson, D.G., 2012. Antarctic circumpolar current's role in the Antarctic ice system: An overview. Palaeogeogr. Palaeoclimatol. Palaeoecol. 335–336, 71–74. https://doi.org/10.1016/J.PALAEO.2011.04.007
- McArthur, J.M., Howarth, R.J., Shields, G.A., Zhou, Y. (2020) Strontium isotope stratigraphy. Geological Time Scale 2020. Elsevier. doi: 10.1016/B978-0-12-824360-2.00007-3
- Mead, G.A., Hodell, D.A., 1995. Controls on the 87Sr/86Sr composition of seawater from the Middle Eocene to Oligocene: Hole 689B, Maud Rise, Antarctica. Paleoceanography 10, 327–346. https://doi.org/10.1029/94PA03069
- Miller, K.G., Wright, J.D., Katz, M.E., Wade, B.S., Browning, J. V., Cramer, B.S., Rosenthal, Y., 2009. Climate threshold at the Eocene-Oligocene transition: Antarctic ice sheet influence on ocean circulation, in: Special Paper of the Geological Society of America. Geological Society of America, pp. 169–178. https://doi.org/10.1130/2009.2452(11)
- Mokadem, F., Parkinson, I.J., Hathorne, E.C., Anand, P., Allen, J.T., Burton, K.W., 2015. High-precision radiogenic strontium isotope measurements of the modern and glacial ocean: Limits on glacial-interglacial variations in continental weathering. Earth Planet. Sci. Lett. 415, 111–120. https://doi.org/10.1016/j.epsl.2015.01.036
- Musumeci, G.; Kramers, J.; Pertusati, P. C. (2000). Early Ordovician terrane accretion along the Gondwanian margin of the East Antarctic Craton: new Pb/Pb titanite ages from the Tonalite Belt, North Victoria Land, Antarctica. Terra nova, 12(1), 35-41. doi/10.1046/j.1365-3121.2000.00271.x
- Ohno, T., Hirata, T., 2007. Simultaneous Determination of Mass-dependent Isotopic Fractionation and Radiogenic Isotope Variation of Strontium in Geochemical Samples by Multiple Collector-ICP-Mass Spectrometry. Anal. Sci. 23, 1275–1280. https://doi.org/10.2116/analsci.23.1275
- Osborne, A.H., Hathorne, E.C., Schijf, J., Plancherel, Y., Böning, P., Frank, M., 2017. The potential of sedimentary foraminiferal rare earth element patterns to trace water masses in the past. Geochemistry, Geophys. Geosystems 18, 1550–1568. https://doi.org/10.1002/2016GC006782
- Pagani, M., Huber, M., Liu, Z., Bohaty, S.M., Henderiks, J., Sijp, W., Krishnan, S., DeConto, R.M., 2011. The role of carbon dioxide during the onset of Antarctic glaciation. Science 334, 1261–4. https://doi.org/10.1126/science.1203909
- Pälike, H., Lyle, M., Nishi, H., Raffi, I., Gamage, K., Klaus, A., Expedition 320/321 Scientists, 2010. Proceedings of the IODP, 320/321. Proc. IODP 320/321.
- Palmer, M.R., 1985. Rare earth elements in foraminifera tests. Earth Planet. Sci. Lett. 73, 285–298. https://doi.org/10.1016/0012-821X(85)90077-9
- Pfuhl, H.A., McCave, I.N., 2005. Evidence for late Oligocene establishment of the Antarctic Circumpolar Current. Earth Planet. Sci. Lett. 235, 715–728. https://doi.org/10.1016/j.epsl.2005.04.025
- Pin, C., Gannoun, A., Dupont, A., 2014. Rapid, simultaneous separation of Sr, Pb, and Nd by extraction chromatography prior to isotope ratios determination by TIMS and MC-ICP-MS. J. Anal. At. Spectrom. 29, 1858–1870. https://doi.org/10.1039/c4ja00169a
- R Development Core Team., 2019. R: A language and environment for statistical computing. R Foundation for Statistical Computing, Vienna, Austria.
- Ravizza, G., Peucker-Ehrenbrink, B., 2003. The marine 187Os/188Os record of the Eocene-Oligocene transition: The interplay of weathering and glaciation. Earth Planet. Sci. Lett. 210, 151–165. https://doi.org/10.1016/S0012-821X(03)00137-7
- Raymo, M.E., Ruddiman, W.F., 1992. Tectonic forcing of late Cenozoic climate. Nature 359, 117–122. https://doi.org/10.1038/359117a0
- Roberts, N.L., Piotrowski, A.M., McManus, J.F., Keigwin, L.D., 2010. Synchronous deglacial overturning and water mass source changes. Science (80-.). 327, 75–78. https://doi.org/10.1126/science.1178068

- Roy, M., van de Flierdt, T., Hemming, S.R., Goldstein, S.L., 2007. 40Ar/39Ar ages of hornblende grains and bulk Sm/Nd isotopes of circum-Antarctic glacio-marine sediments: Implications for sediment provenance in the southern ocean. Chem. Geol. 244, 507–519. https://doi.org/10.1016/j.chemgeo.2007.07.017

- Sarkar, S., Basak, C., Frank, M., Berndt, C., Huuse, M., Badhani, S., Bialas, J., 2019. Late Eocene onset of the Proto--Antarctic Circumpolar Current. Sci. Rep. 9, 10125. https://doi.org/10.1038/s41598-019-46253-1

- Sauermilch, I., Whittaker, J.M., Klocker, A., Munday, D.R., Hochmuth, K., LaCasce, J.H., Bijl, P., 2019. Tectonic Gateway Driven Cooling of Antarctica with High Resolution Ocean Models, in: American Geophysical Union, Fall Meeting 2019. Vienna, pp. PP11B-02.

- Scher, H.D., Martin, E.E., 2004. Circulation in the Southern Ocean during the Paleogene inferred from neodymium isotopes. Earth Planet. Sci. Lett. 228, 391–405. https://doi.org/10.1016/J.EPSL.2004.10.016

- Scher, H.D., Martin, E.E., 2006. Timing and climatic consequences of the opening of Drake Passage. Science 312, 428–30. https://doi.org/10.1126/science.1120044

- Scher, H.D., Martin, E.E., 2008. Oligocene deep water export from the North Atlantic and the development of the Antarctic Circumpolar Current examined with neodymium isotopes. Paleoceanography 23, n/a-n/a. https://doi.org/10.1029/2006PA001400

- Scher, H.D., Delaney, M.L., 2010. Breaking the glass ceiling for high resolution Nd isotope records in early Cenozoic paleoceanography. Chem. Geol. 269, 329–338. https://doi.org/10.1016/J.CHEMGEO.2009.10.007

- Scher, H.D., Bohaty, S.M., Zachos, J.C., Delaney, M.L., 2011. Two-stepping into the icehouse: East Antarctic weathering during progressive ice-sheet expansion at the Eocene-Oligocene transition. Geology 39, 383–386. https://doi.org/10.1130/G31726.1

- Scher, H.D., Bohaty, S.M., Smith, B.W., Munn, G.H., 2014. Isotopic interrogation of a suspected late Eocene glaciation. Paleoceanography 29, 628–644. https://doi.org/10.1002/2014PA002648

- Scher, H.D., Whittaker, J.M., Williams, S.E., Latimer, J.C., Kordesch, W.E.C., Delaney, M.L., 2015. Onset of Antarctic Circumpolar Current 30 million years ago as Tasmanian Gateway aligned with westerlies. Nature 523, 580–583. https://doi.org/10.1038/nature14598

- Scher, H., 2017. Carbon–ocean gateway links. Nat. Geosci. 10, 164–165. https://doi.org/10.1038/ngeo2895

- Shackleton, N.J., Kennett, J.P., 1975. Paleotemperature History of the Cenozoic and the Initiation of Antarctic Glaciation: Oxygen and Carbon Isotope Analyses in DSDP Sites 277, 279 and 281, in: Initial Reports of the Deep Sea Drilling Project, 29. U.S. Government Printing Office. https://doi.org/10.2973/dsdp.proc.29.117.1975

- Stickley, C.E., Brinkhuis, H., Schellenberg, S.A., Sluijs, A., Röhl, U., Fuller, M., Grauert, M., Huber, M., Warnaar, J., Williams, G.L., 2004. Timing and nature of the deepening of the Tasmanian Gateway. Paleoceanography 19, n/a-n/a. https://doi.org/10.1029/2004PA001022

- Stow, D.A.V., 2001. Deep-Sea Sediment Drifts. Encycl. Ocean Sci. 80–89. https://doi.org/10.1016/B978-012374473-9.00422-7

- Straume, E.O., Gaina, C., Medvedev, S., Nisancioglu, K.H., 2020. Global Cenozoic Paleobathymetry with a focus on the Northern Hemisphere Oceanic Gateways. Gondwana Res. https://doi.org/10.1016/j.gr.2020.05.011

- Thomas, D.J., 2004. Evidence for deep-water production in the North Pacific Ocean during the early Cenozoic warm interval. Nature 430, 65–68. https://doi.org/10.1038/nature02639

- Toumoulin, A., Donnadieu, Y., Ladant, J.-B., Batenburg, S. J., Poblete, F., & Dupont-Nivet, G. (2020). Quantifying the effect of the Drake Passage opening on the Eocene Ocean. Paleoceanography and Paleoclimatology, 35, e2020PA003889. doi.org/10.1029/2020PA003889

- Tripati, A. K., J. Backman, H. Elderfield, and P. Ferretti (2005), Eocene bipolar glaciation associated with global carbon cycle changes, Nature, 436, 341– 346, doi:10.1038/nature03874.

- Vahlenkamp, M., Niezgodzki, I., De Vleeschouwer, D., Bickert, T., Harper, D., Kirtland Turner, S., Lohmann, G., Sexton, P., Zachos, J., Pälike, H., 2018. Astronomically paced changes in deep-water circulation in the western North Atlantic during the middle Eocene. Earth Planet. Sci. Lett. 484, 329–340. https://doi.org/10.1016/j.epsl.2017.12.016
- van de Flierdt, T., 2011. Continental weathering through the onset of Antarctic glaciation. Geology. https://doi.org/10.1130/focus042011.1
- van de Flierdt, T., Goldstein, S.L., Hemming, S.R., Roy, M., Frank, M., Halliday, A.N., 2007. Global neodymium-hafnium isotope systematics - revisited. Earth Planet. Sci. Lett. 259, 432–441. https://doi.org/10.1016/j.epsl.2007.05.003
- Vito, M., Muggeo, R., 2003. Estimating regression models with unknown break-points. Stat. Med. 22, 3055–3071.
- Weber M., Lugli F., Jochum K.P., Cipriani A., Scholz D., 2017. Calcium carbonate and phosphate reference materials for monitoring bulk and microanalytical determination of Sr isotopes. Geostandards and Geoanalytical Research, 42(1), 77-89, doi: 10,1111/ggr.12191.
- Wright, N.M., Scher, H.D., Seton, M., Huck, C.E., Duggan, B.D., 2018. No Change in Southern Ocean Circulation in the Indian Ocean From the Eocene Through Late Oligocene. Paleoceanogr. Paleoclimatology 33, 152–167. https://doi.org/10.1002/2017PA003238
- Yeghicheyan D., Carignan J., Valladon M., Bouhnik Le Coz M., Samuel J., BenBakkar,M., Bruguier O., Keller F., Pin C., Pourtales S., Hénin O., Macé J., Morin N., Guilmette C., Marin L., 2003. The new carbonate reference material CAL-S : preliminary results. Congres Geoanalysis 2003.
- Zachos, J.C., Opdyke, B.N., Quinn, T.M., Jones, C.E., Halliday, A.N., 1999. Early cenozoic glaciation, antarctic weathering, and seawater 87Sr/86Sr: is there a link? Chem. Geol. 161, 165–180. https://doi.org/10.1016/S0009-2541(99)00085-6
- Zachos, J., Pagani, M., Sloan, L., Thomas, E., Billups, K., 2001. Trends, rhythms, and aberrations in global climate 65 Ma to present. Science 292, 686–93. https://doi.org/10.1126/science.1059412
- Zhang, J., Nozaki, Y., 1996. Rare earth elements and yttrium in seawater: ICP-MS determinations in the East Caroline, Coral Sea, and South Fiji basins of the western South Pacific Ocean. Geochim. Cosmochim. Acta 60, 4631–4644. https://doi.org/10.1016/S0016-7037(96)00276-1
- Zhang, Y., Huck, T., Lique, C., Donnadieu, Y., Ladant, J.B., Rabineau, M., Aslanian, D., 2020. Early Eocene vigorous ocean overturning and its contribution to a warm Southern Ocean. Clim. Past 16, 1263–1283. https://doi.org/10.5194/cp-16-1263-2020

Acknowledgements

F.H. thanks IODP France for his postdoc fellowship and post cruise-support. Authors also acknowledge M. Henry, for his help in clean laboratory, S. Mounic for her assistance on the TIMS and A. Marquet on the ICP-MS. J. Sonke is thanked for his advices and discussions. Authors are grateful to the two anonymous reviewers and to Prof. B. Kamber for their important contributions that significantly improved this manuscript. V.C. would like to pay tribute to Jan for his conviviality, stimulating, and open-minded supervision during the course of her Ph.D. fellowship at the University of Bern. Thank you very much for all your support, advise and kindness.

Figure captions

Figure 1: (a, b) Compilation of Drake Passage gateway opening ages reported in literature (Latimer and Filippelli, 2002; Lawver and Gahagan, 2003; Livermore et al., 2005, 2007; Pfuhl and McCave, 2005; Brown et al., 2006; Eagles et al., 2006; Scher and Martin, 2006; Barker et al., 2007; Lagabrielle et al., 2009; Egan et al., 2013; Borrelli et al., 2014; Scher et al., 2015; Sarkar et al., 2019) (soft colours are for shallow depth aperture and dark colours for deep aperture, curves in b are kernel density obtained using the Past 3 software (Hammer et al., 2001). The deep aperture of the Tasmanian gateway between 35.5 and 33.5 Ma (Stickley et al., 2004) is also reported (in brown). The polar-centered map (Martinson, 2012) schematizes the clockwise Antarctic Circumpolar Current following the Tasmanian and Drake Passage gateways opening (in blue). Submarine areas above 3000 m depth are represented in light grey and land in black. Studied ODP/IODP legs are also reported as well as the Agulhas Ridge and the Kerguelen Plateau locations, which are further considered in the discussion.

Figure 2: Age models for samples (large coloured symbols) from the IODP Leg 320 Hole 1334 C (a) and ODP Leg 113 Hole 689 B (b). Calibrations are based on a synthesis of magnetostratigraphic and biostratigraphic data symbolized by black dots (Barker et al., 1988; Pälike et al., 2010). The age data of the Leg 113 have been updated according to the Geological Timescale 2012 (GTS2012). Regressions are computed using the packages changepoint (Killick and Eckley, 2014) and segmented (Vito and Muggeo, 2003) on the R software (R Development Core Team., 2019). Uncertainties (represented in shaded colours) correspond to the 95 % confident interval of regressions.

Figure 3: Secondary electrons SEM microphotographs of hand-picked foraminifera (a, b, c, d) and residual fractions remaining after the cleaning and the acid dissolution procedure (e, f). The samples include planktonic (Globigerina; a,b) and benthic (Nodosaria and Gyroidinoides, respectively c and d) foraminifera. No evidence of secondary calcite recrystallization is noticeable, attesting of the pristine character of tests. (e) Residue after cleaning and dissolution procedure showing undissolved and discarded quartz grains (Qtz), amorphous silica from radiolarian tests (Si), pyrite (Pyr) and clay minerals (Clays). (f) Undissolved and discarded clay platelets.

Figure 4: Clay-$CaC0_3$ mixing models for Si/Ca (a) and Al/Ca (b) (µmol/mol) ratios attesting of the absence of noticeable clay contamination after our cleaning and digestion protocol (always less than 0.005 % of potential clay contamination, less than 0.002 % for 95% of the samples). Major element contents of illite, smectite and kaolinite used for calculations are from Deer et al. (2013). Box-and-whiskers plots showing the distribution of foraminifera samples from the 1334C (yellow) and 689B (red) sites were obtained using the Past3 software (Hammer et al., 2001).

Figure 5: PAAS normalized REE spectra of the planktonic and benthic foraminifera tests from site 1334C (a) and 689B (b). PAAS normalizing values are from Barth et al. (2000) with Tm from Kamber et al. (2005). Modern seawater REE (x 10^6) spectrum are represented for comparison (data are from Grenier et al., 2013 for the equatorial PO and from Hathorne et al., 2014 for the SAO).

Figure 6: Evolution of Ce/Ce^*_N (a), Mg/Ca (b) and $^{87}Sr/^{86}Sr$ ratios (c) recorded by the benthic (light colour) and planktonic (dark colour) foraminifera from the studied sites 689B and 1334C along the Eocene-Oligocene interval (EOT). Because it has been shown that planktonic foraminifera could exchange REE with seawater along their rain-down through the water column and once on the seafloor (e.g. Roberts et al., 2010; Osborne et al., 2017), temporal evolutions of their Ce/Ce anomaly cannot be interpreted as signing surface seawater redox state evolutions but an integrated signal of the whole water column. PAAS normalizing values are from Barth et al. (2000). The Mg/Ca data are compared to the benthic foraminifera $\delta^{18}O$ data of (Kennett and Stott, 1990) of the site 689B (ODP Leg 113). Normalized variation curves are normalized prime derivatives of smoothing spline functions of the $^{87}Sr/^{86}Sr$ data generated with the R software (R Development Core Team., 2019). Error bars for both ages and $^{87}Sr/^{86}Sr$ ratios are similar to symbol size. The red and the yellow domains drawn for sites 689B and 1334C represent the envelopes of the maximal error bars. Compiled $^{87}Sr/^{86}Sr$ data for the SO are from (Barrera et al., 1991; Mead and Hodell, 1995; Zachos et al., 1999; Scher and Martin, 2004).*

Figure 7: Schematic representation of the hypothesized mixed layered depth evolution at Maud Rise (SAO) in response to Drake Passage gateway opening based on numerical modelling studies of Ladant et al. (2018) and Zhang et al. (2020) and on our data (Fig. 6). This stratification scenario fits with (1) our Mg/Ca data indicating surface water warming and bottom water remaining cold between 31 and 27 Ma and (2) bottom SAO seawater oxygenation indicated by negative Ce

anomalies increase along the 31-26 Ma interval, up to reach similar value to deep pacific waters. SAO/PO seawater masses homogenization is also suggested by Sr isotopes ratios that are dissociated before 31 Ma and identical after. Approximate paleo-depths are from Barker et al. (1988).

Figure 8: (a) Compilation of benthic foraminifera $\delta^{18}O$ for the high latitudes of the Southern Ocean (e.g., Maud Rise and Kerguelen Plateau, in red), Southern Atlantic Ocean (in grey), and Pacific Ocean (in yellow) by Cramer et al. (2009). (b) Compilation of published fossil fish teeth ε_{Nd} data for the Maud Rise (in red, site 689), the Kerguelen Plateau (in green, sites 738, 744, 748), the Agulhas Ridge (in blue, site 1090) and the Pacific Ocean (in yellow, sites 192, 277, 464, 465, 883, 884, 1124, 1168, 1172, 1208, 1209, 1211) during the Eocene-Oligocene interval (Thomas, 2004; Scher and Martin, 2004, 2006, 2008; Scher and Delaney, 2010; Scher et al., 2011, 2014, 2015; Hague et al., 2012; Huck et al., 2017; Wright et al., 2018). Punctual weathering flux increases are from Scher et al. (2011, 2014). Clay minerals changes are from Ehrmann and Mackensen (1992) and Diekmann et al. (2004).

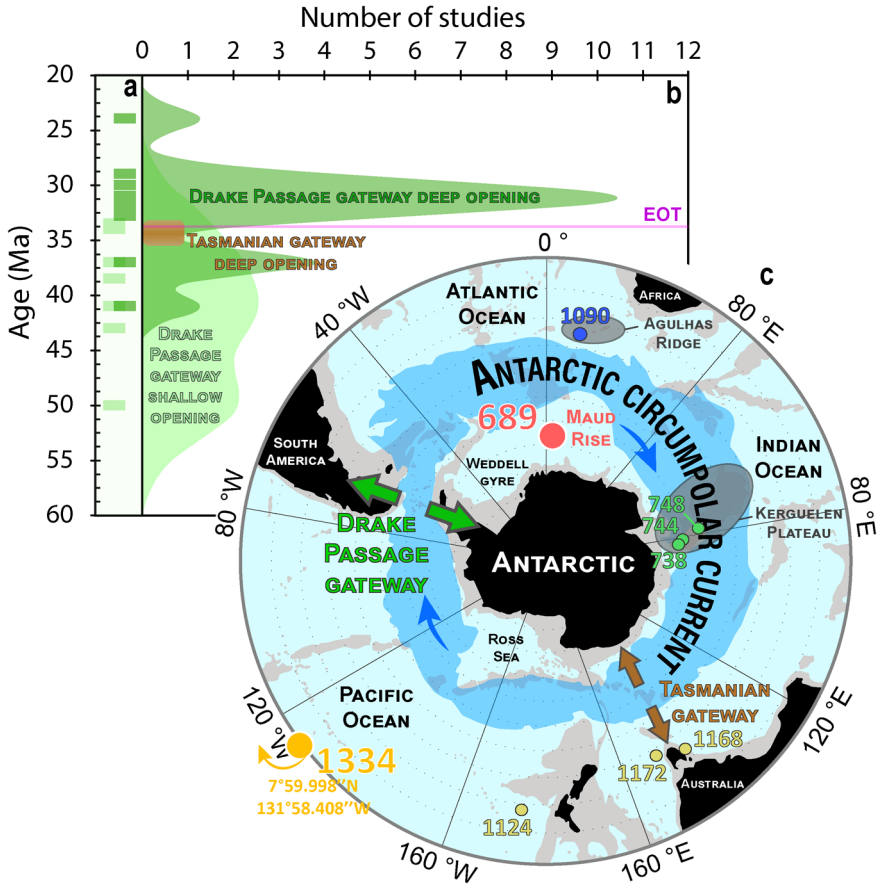

Figure 1

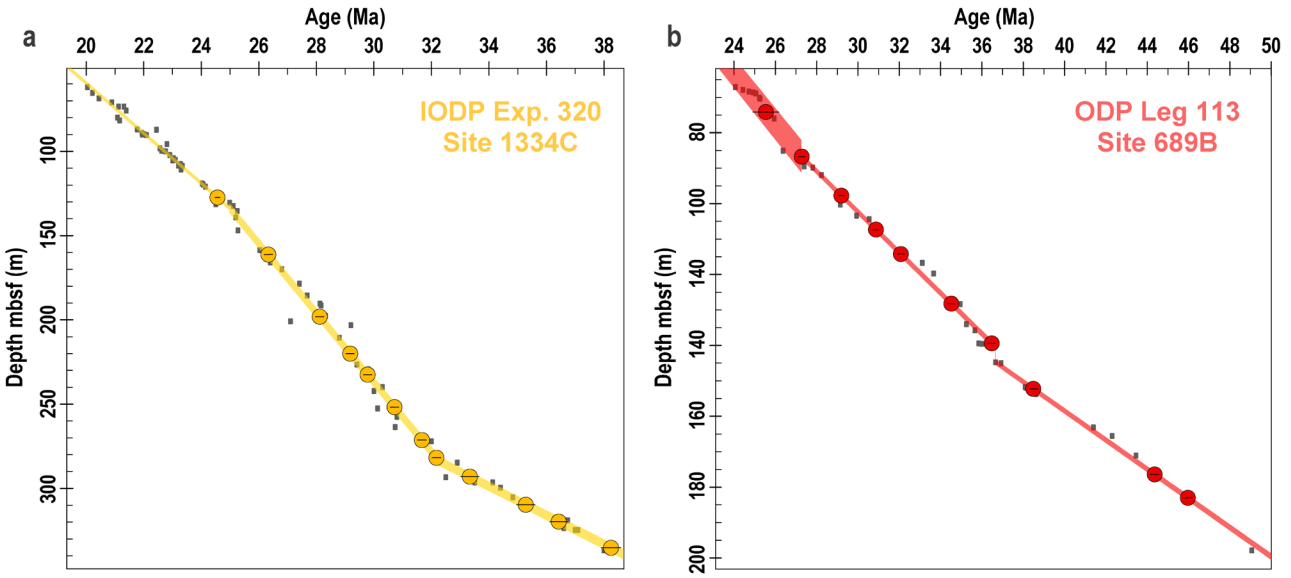

Figure 2

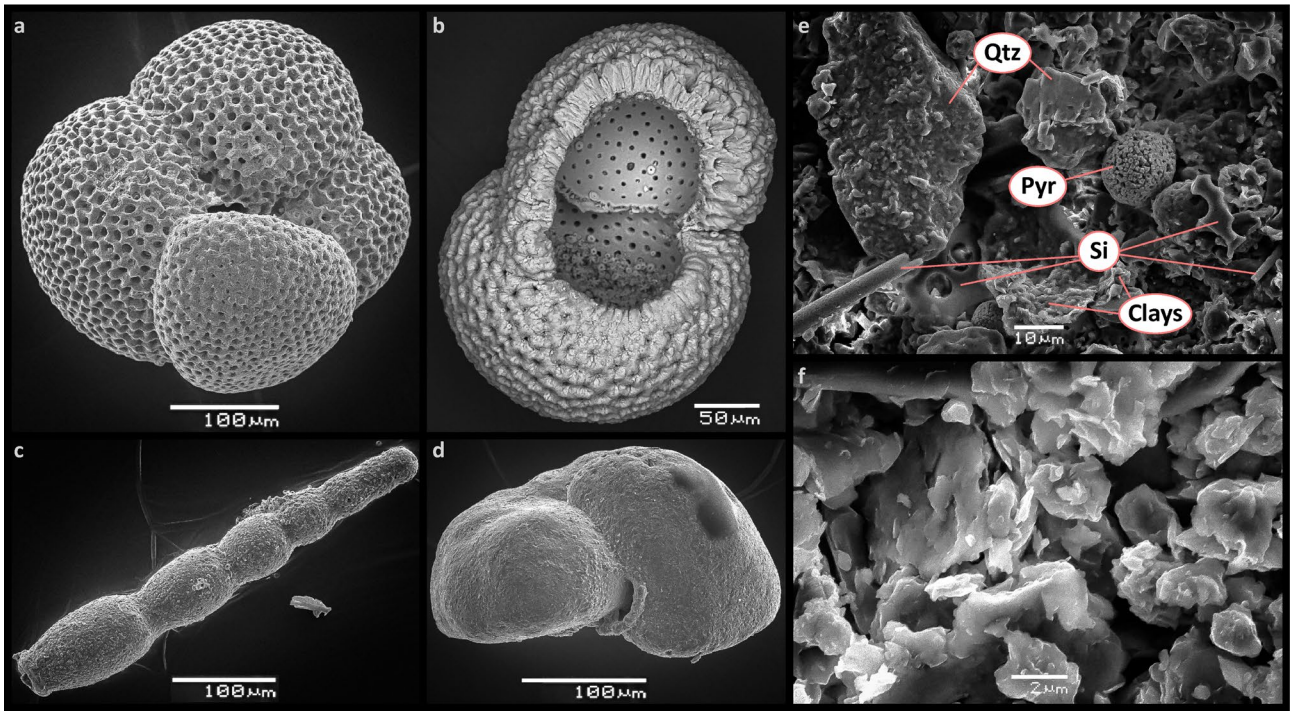

Figure 3

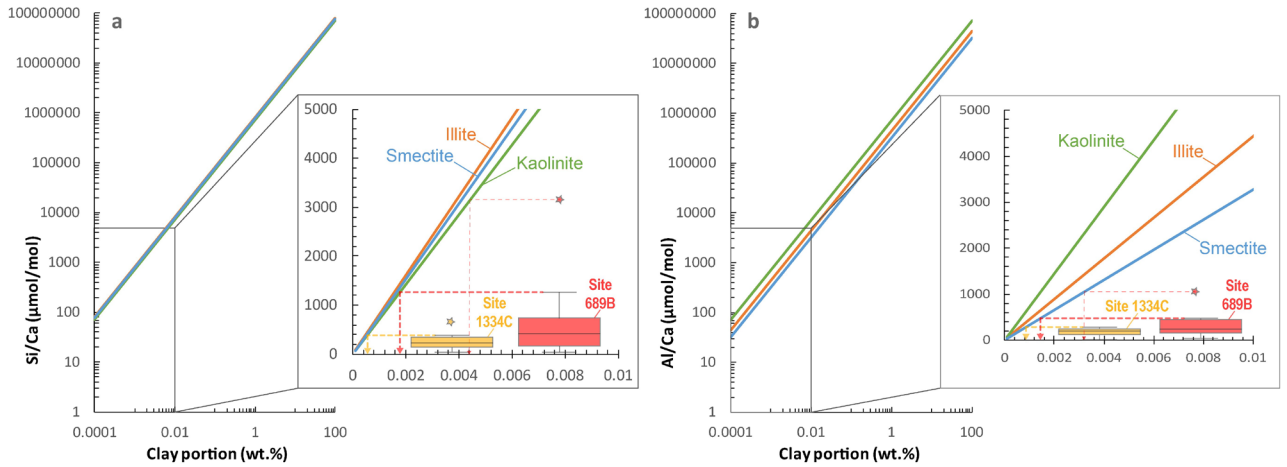

Figure 4

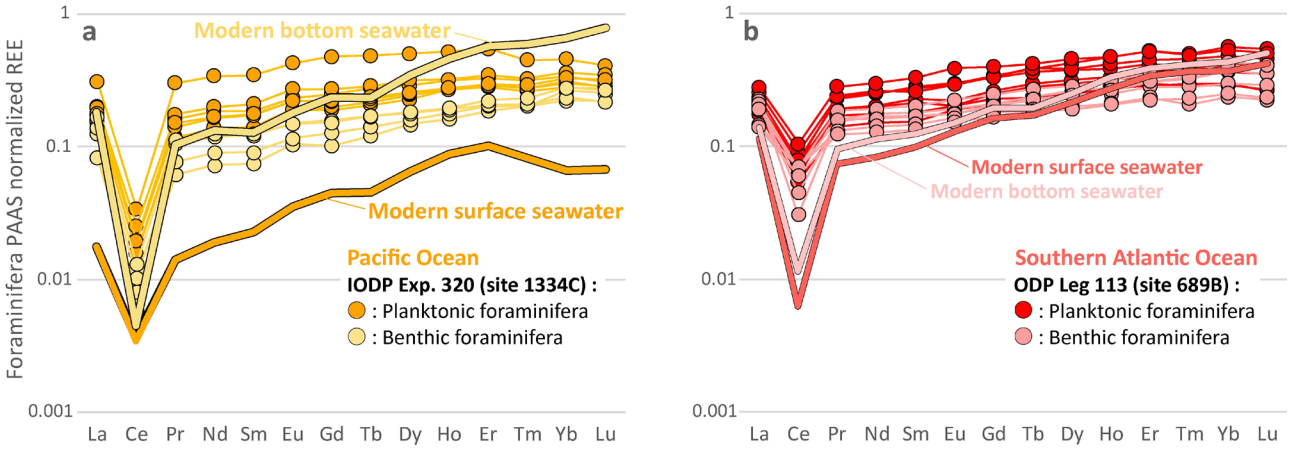

Figure 5

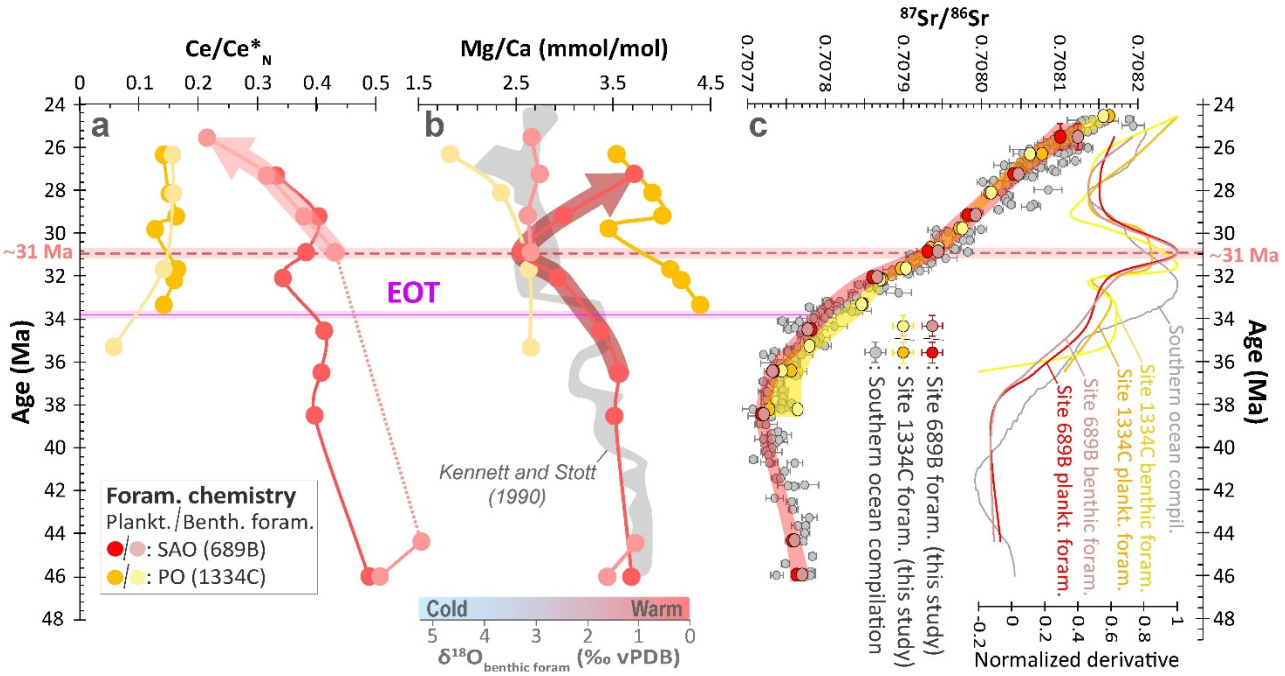

Figure 6

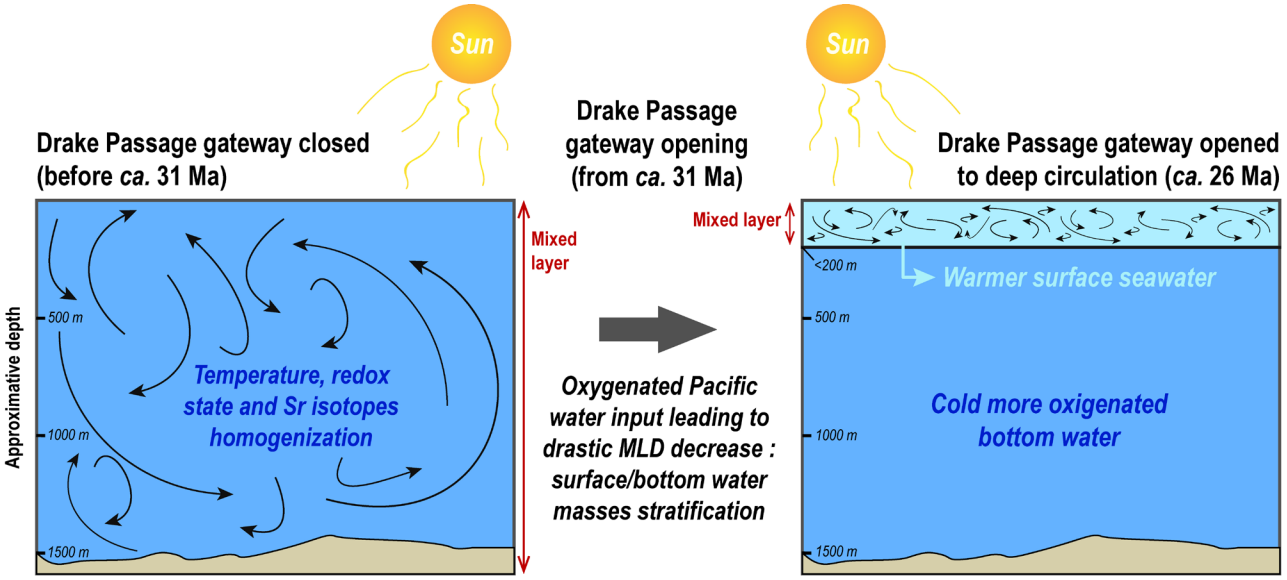

Figure 7

947

948

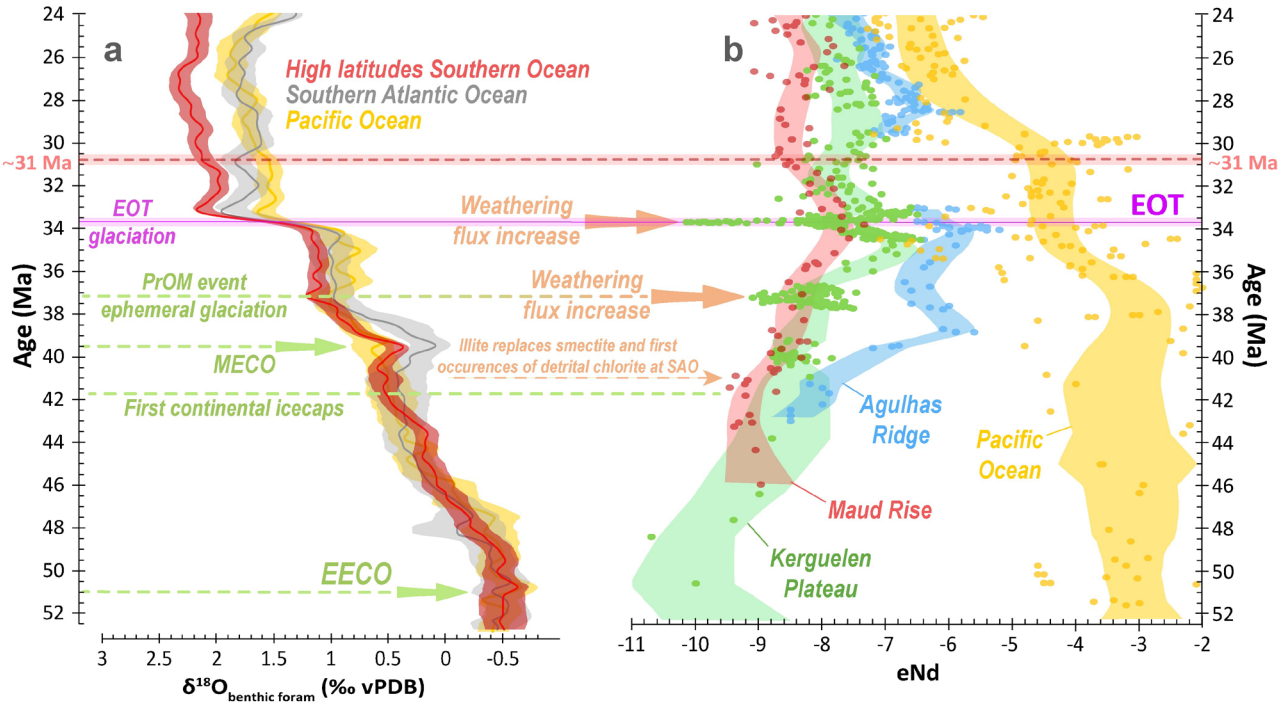

949

950 *Figure 8*